AD-A129 624 ANALYSIS OF NOVEL SUPERCONDUCTING MAGNETOMETER WITH SUPERIOR NOISE AND COUPLING PROPERTIES(U) LUTECH INC BERKELEY CA C D TESCHE NOV 81 N00014-80-C-0611 1/1

UNCLASSIFIED F/G 14/2 NL

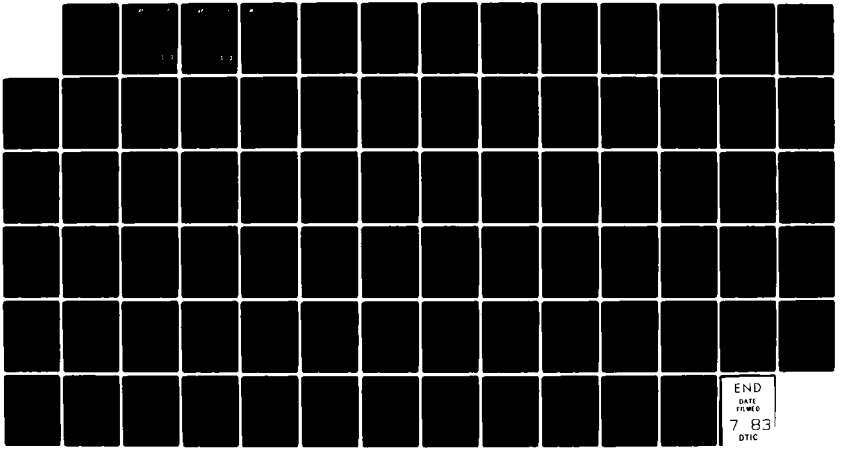

END
DATE FILMED
7 83
DTIC

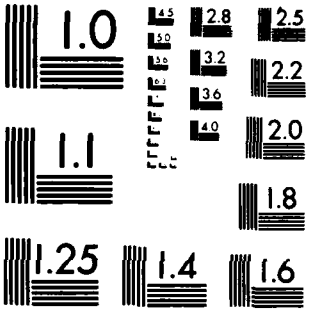

MICROCOPY RESOLUTION TEST CHART
NATIONAL BUREAU OF STANDARDS-1963-A

LuTech, Inc.

NR 319-154

(1)

LuTech, Inc.

ANALYSIS OF A NOVEL SUPERCONDUCTING
MAGNETOMETER WITH SUPERIOR
NOISE AND COUPLING PROPERTIES

LuTech, Inc. Phone: (415) 843-1504
P.O. Box 1263, 127 University Avenue, Berkeley, California 94701

ANALYSIS OF A NOVEL SUPERCONDUCTING MAGNETOMETER WITH SUPERIOR NOISE AND COUPLING PROPERTIES

Interim Report

by

C.D. Tesche

NOV. 1981

Submitted to:

Office of Naval Research
Physical Sciences Division

Submitted by:

LuTech, Inc.
P.O. Box 1263
Berkeley, CA 94701

N00014-82-C-0611

TABLE OF CONTENTS

LIST OF FIGURES

I. INTRODUCTION

There is considerable interest in the development of extremely sensitive superconducting magnetometers for the detection of changes in magnetic field intensity. The most sensitive detectors developed up to this time are thin film dc SQUID magnetometers.[1] The dc SQUID consists of a superconducting loop interrupted by two Josephson junctions.[2] If the junctions are biased near the critical current by an externally applied dc bias current, the voltage across the junctions becomes a sensitive function of the flux threading the loop. Thus, the dc SQUID acts like a flux to voltage transducer.

The resolution of the dc SQUID magnetometer is determined predominately by three factors.[3,4] First, the Josephson junctions employed in the device must be non-hysteretic. As a result, the thin film tunnel junctions typically used in the device are externally shunted by a normal resistance. The Johnson noise associated with this resistance produces fluctuations in the voltage across the SQUID. This noise can be referred to the input as an effective flux noise, S_Φ. A useful figure of merit is then the energy factor $S_E = S_\Phi/2L$, where L is the SQUID loop inductance. In the usual mode of operation, the incident magnetic field is coupled into the SQUID through a superconducting transformer. The pick-up coil is connected in a series with a coupling coil which is inductively coupled to the SQUID loop. In this case, the minimum detectable change in magnetic field energy stored in the pick-up coil is proportional to the energy factor S_E. For conventional dc SQUIDs, the energy factor is determined by the temperature T, the loop inductance L, and junction capacitance C, $S_E \propto k_B T \sqrt{LC}$. The ultimate resolution for quantum noise limited devices appears to be $S_E \approx \hbar$.[5]

The second factor which limits the resolution of dc SQUID magnetometers is the presence of 1/f noise at the output of the device.[3] The source of this noise is not well understood. However, it is likely that the dominant source is related to low frequency thermal fluctuations within the Josephson junction.[6,7,8] These fluctuations increase in importance

as the effective junction volume is reduced. Since the effective volume scales with the junction capacitance, attempts to reduce the energy factor at low frequencies by decreasing the junction capacitance have failed. In fact, for the most sensitive devices with $S_E \sim h$, 1/f noise is the dominant noise source at frequencies $f \gtrsim$ 10-100 KHz.[8]

The third factor which limits the resolution of the dc SQUID magnetometer is the intrinsic low loop inductance of the device. For example, the maximum practical loop inductance for devices operated at 4K is $L \sim$ nH.[4] SQUIDs with energy factors S_E approaching $\hbar$ have been fabricated with loop inductance $L \sim$ pH.[9] However, the magnetic field resolution depends not only on the energy factor S_E, but also on the effective area of the pick-up coil. Since the pick-up coil inductance must be matched to the inductance of the coupling coil to the SQUID, the magnetic field resolution is limited by the coupling efficiency between the SQUID loop and the coupling coil. As a result, planar dc SQUIDs with loop inductance $L \lesssim$ pH show little promise as sensitive detectors of magnetic field intensity.

Recently, a novel superconducting device related to the dc SQUID has been suggested by Ho Jung Paik.[10] In this device, the single dc SQUID loop is replaced by a double loop structure. In this configuration, a "SQUID" loop containing two Josephson junctions and a superconducting "coupling" loop are connected in parallel with a shorting capacitance. It has been suggested that the behavior of this device will be closely related to the ordinary dc SQUID. In particular, a heuristic calculation suggests that the coupling properties of the device will be determined by the coupling loop inductance, whereas the energy factor will be determined by the SQUID loop inductance.[10] Thus, by decreasing the SQUID loop inductance without sacrificing the ability to couple efficiently to large input coils.

In this report we describe the results of a detailed investigation of the double loop SQUID magnetometer. We begin by presenting a thermal activation model for the DC SQUID which supplements the original numerical simulations of the device. The model is particularly useful for deriving the behavior of the device at low bias currents. The equations of motion

for the dc SQUID are then compared with a lumped circuit element model for the double loop SQUID. A relationship between the double loop and conventional SQUID characteristics in the absence of noise is described. Direct numerical simulations of the double loop device are then performed. Noise free characteristics are computed as a function of the coupling loop resonant frequency, the bias current and the applied flux. Noise rounded characteristics are then generated. An approximate expression for the flux resolution as a function of the total loop inductance is determined. A model is developed for conventional and double loop SQUID magnetometers. The model includes explicitly the effects of the input circuit on the SQUID characteristics. The resolution of superconducting and lossy double loop magnetometers is calculated as a function of the signal frequency and the input and SQUID circuit parameters.

Some of the basic results reported for the isolated double loop SQUID were computed in conjunction with a project on the analysis of double loop linear amplifier performed for the National Science Foundation under Grant DAR-8009388.

II. MODEL FOR THE CONVENTIONAL DC SQUID

A. Numerical Simulation of Lumped Circuit Element Model

The conventional dc SQUID[1] consists of a superconducting loop interrupted by two Josephson junctions.[2] A lumped circuit element model for the device is shown in Figure 1.[4] The SQUID is biased at constant current I. The average voltage $\overline{V}$ across the SQUID output is then a periodic function of the flux Φ_a applied to the loop inductance L. The RSJ model (Fig. 2(a)) is used to describe the behavior of the junctions.[12] The junction critical currents are $I_{01} = (1 - \alpha)I_o$ and $I_{02} = (1 + \alpha)I_o$, where α is the asymmetry parameter. The junction shunt resistance is R. We consider the limit $\beta_c = RC/(\Phi_o/2\pi I_o R) << 1$.

The differential equations describing the development of the quantum mechanical phase differences δ_1 and δ_2 across the Josephson junctions are then[4]

$$\left(\frac{\Phi_o}{2\pi R}\right)\frac{d\delta_1}{dt} = I/2 - J - I_o\,(1 - \alpha)\,\sin\,\delta_1 + V_{N1}/R, \tag{1}$$

$$\left(\frac{\Phi_o}{2\pi R}\right)\frac{d\delta_2}{dt} = I/2 + J - I_o(1 + \alpha)\,\sin\,\delta_2 + V_{N2}/R, \tag{2}$$

where V_{N1} and V_{N2} are the Johnson noise voltages associates with the shunt resistances. The circulating current J is related to the junction phase differences by the quantization of the fluxoid

$$LJ = (\delta_1 - \delta_2)/2\pi - \Phi_a \tag{3}$$

where Φ_a is the quasistatic flux applied to the ring. The voltage developed acorss the junctions is

$$V = \frac{\Phi_o}{4\pi}\left(\frac{d\delta_1}{dt} + \frac{d\delta_2}{dt}\right) . \tag{4}$$

The equations of motion have been solved by numerical simulation.[4] The voltage V(t) and circulating current J(t) are computed as a function of the bias current I and applied flux Φ_a by stepwise integration of Eqs. 1-4. The time averaged voltage $\bar{V}(\Phi_a)$, forward transfer function $\partial\bar{V}/\partial\Phi_a$, voltage noise power spectral density $S_V(f)$, circulating current noise spectral density $S_J(f)$, and correlation noise spectral density $S_{VJ}(f)$ are then computed. The effective flux noise spectral density at the input is $S_\Phi = S_V/(\partial V/\partial\Phi_a)^2$. In most cases, we are interested in the constant low frequency component, S_Φ^o, at frequencies $f \ll I_o R/\Phi_o$.

The numerical simulation yields results which are in good agreement with observed characteristics for bias currents $I \gtrsim 2I_o$. However, the simulation is fairly tedious. In addition, at bias currents $I \ll 2I_o$, numerical simulation is not practical. Furthermore, the simulation does not provide a clear intuitive framework upon which further investigation can be based.

B. Thermal Activation Model

We present a thermal activation model for the conventional dc SQUID which provides a clear, intuitive description of the behavior of the device. The model depends on the fact that the equations of motion (Eqs. 1-4) can be derived from a potential $U(\delta_1,\delta_2)$. This is not a trivial statement. In fact, the equations of motion of numerous interesting devices cannot be related to a potential field. The double loop SQUID is an example of such a device. However, both the single resistively shunted Josephson junction and the rf SQUID can be described by a potential.[14,15,16,17] For example, the equations of motion for the single current biased Josephson junction (RSJ model) are

$$\beta_c \frac{d^2\delta}{d\theta^2} + \frac{d\delta}{d\theta} = -\frac{\partial u}{\partial\delta} + v_N \qquad (5)$$

where $u(\delta) = -\cos\delta - i\delta$. (6)

In these equations, the bias current $I = iI_0$, and the voltage across the junction $V = (I_0R)v = (I_0R)d\delta/d\theta$. The dimensionless time $\theta = t/(\Phi_0/2\pi I_0R)$. At bias currents $i < 1$, the potential consists of a one dimensional chain of wells separated by barriers (the "washboard" potential, Fig. 2(b)) develops in time like the coordinate of a particle moving in a viscous medium within the wells. The random Johnson noise voltages v_N cause the particle to make transitions over the barrier between the wells. A voltage pulse is generated in the process. Thus, the time averaged voltage is proportional to the average rate of escape over the barriers.

At low temperatures ($k_BT << 2eI_0R$), the power spectral density of the thermal fluctuations in the voltage across the shunt resistor will roll off like $S_N(\omega) \sim \hbar\omega \exp(-\hbar\omega/k_BT)$. In this regime, the dominant source of voltage fluctuations across the single junction will be produced by the detailed quantum mechanical behavior of the junction. The investigation of this behavior is a subject of consideration interest at this time.

The conventional dc SQUID equations can be related to the equations of motion of a particle moving in a two dimensional potential field,

$$\beta_c \frac{d^2\delta_k}{dt^2} + \frac{d\delta_k}{dt} = -\frac{\partial u}{\partial \delta_k} + v_k \qquad k = 1, 2 \tag{7}$$

where the potential $u(\delta_1, \delta_2)$ satisfies

$$u(\delta_1,\delta_2) = -\cos\delta_1 - \cos\delta_2 - (\delta_1 + \delta_2)\, i/2 + \pi\beta j^2/2 \tag{8}$$

and

$$j = (\delta_1 - \delta_2 - 2\pi\phi_a)/\pi\beta. \tag{9}$$

The junction parameters are critical current I_0, capacitance C and shunt resistance R. the voltage developed across the junctions, $V = vI_0R$, is a function of the dc bias current $I = iI_0$ and the applied flux $\phi_a = \phi_a\phi_0$.

The screening factor is $\beta = 2LI_o/\Phi_o$ and $\beta_c = 2\pi I_o R^2 C/\Phi_o$. We shall be interested in the solution to these equations in the overdamped limit, $\beta_c << 1$.

Equations 7-9 are a set of classical equations of motion for a particle moving in a two dimensional potential field. The form of the potential $u(\delta_1,\delta_2)$ is similar to the one dimensional field for the single current biased junction. The potential consists of a family of wells located within a low potential trough. An example is plotted in Figure 3 for bias current $i = 0$, applied flux $\phi_a = 0.5$ and screening factor $\beta = 1$. At low bias currents in the absence of noise, the particle velocity will be damped out. Thus, the particle will settle into a single well. As the bias current is increased, the potential trough is tipped and the barrier between successive wells is decreased. At some critical current, i_c, which is a function of the applied flux ϕ_a, the barrier vanishes. At this point, the particle propagates freely down the potential trough. Since the voltage is proportional to the direct sum of the components of the particle velocity, a voltage develops across the SQUID (see Fig. 4).

In the presence of noise (v_{N1}, $v_{N2} \neq 0$), the particle undergoes Brownian motion in the potential field. At bias currents $i < i_c(\phi_a)$, the particle motion occurs predominately within the potential well. However, the particle will occasionally make a classical transition over the barrier. The thermal activation of the particle from one well to the next produces an average voltage across the SQUID even at bias currents $i < i_c(\phi_a)$ (see Fig. 5). The voltage pulse produced as the particle escapes from the well is usually accompanied by a pulse in the circulating current around the SQUID as each of the phase differences advances by 2π. Fluctuations in the number of pulses per unit time generate low frequency noise in the voltage and circulating current. In addition, noise is generated by the random motion of the particle in the wells. This source of noise is most pronounced in the low frequency current noise at bias currents $i << i_c(\phi_a)$. Motion within the well does not contribute substantially to the low frequency voltage noise. An example of current and voltage low frequency noise spectral densities as a function of bias current are plotted in Fig. 6 and Fig. 7. Near the critical current, the random generation of the

current and voltage pulses is the dominant source of noise. Since the current and voltage pulses are coincident, the two noise components are strongly correlated (see Fig. 8).

The conventional dc SQUID I-V characteristics and noise spectral densities can be computed directly from the form of the potential u for values of bias current $i \lesssim i_c$. The probability of making a single transition over a barrier height Δu in the overdamped limit ($\beta_c \ll 1$) depends exponentially on the barrier height,

$$P = \frac{1}{2\pi} \frac{C_{w1} C_{w2} C_{s1}}{|C_{s2}|} \exp\left(-\frac{\Delta u}{\Gamma}\right) \tag{10}$$

where C_{w1}, C_{w2}, and C_{s1}, $|C_{s2}|$ are the curvatures of the well and saddle expressed in normal coordinates. The factor Γ is the ratio of the thermal energy to the intrinsic energy of the junction, $\Gamma = 2\pi k_B T / I_o \Phi_o$.

The motion of the particle down the chain of well is analogous to the action of a non-paralyzable counter. The occurence of an event at the counter corresponds to the escape of the particle over the barrier. The counter deal time corresponds to the transit time τ over the barrier. The times between successive pulses are the sum of the independent, randomly distributed transition and pulse times. The transition times (time in the wells) are exponentially distributed with mean $1/p$ and variance $1/p^2$. We assume that the variance in the pulse time $\tau_v \ll 1/p^2$. The mean number of pulses arriving in unit time is $\bar{n} = 1/\mu$ and the variance in n is $(\Delta n)^2 = \sigma^2/\mu^3$, where σ^2 is the sum of the variances in the transition time and μ is the sum of the means.[22]

Thus, the effective transition rate is

$$r = p/(1 + p\tau) \tag{11}$$

and the variance in the number of transitions per unit time is

$$(\Delta n)^2 = \frac{p}{(1 + p\tau)^3} \tag{12}$$

The average voltage is

$$\bar{v} = 2\pi r = \frac{2\pi p}{(1 + p\tau)} \tag{13}$$

and the low frequency voltage spectral density generated by fluctuations in the number of pulses is

$$S_v^o = 2(2\pi)^2 \Delta n^2 = 2(2\pi)^2 \frac{p}{(1 + p\tau)^3} \quad , \qquad f << f_J . \tag{14}$$

As mentioned previously, the circulating current noise, S_j^o, arises from two sources. There is a contribution generated by the motion of the particle from one well to another, and a contribution from motion within the well. In the first case, the current pulse $j_p = \int (j - j_w)d\theta$, where the limits of integration are taken from the bottom of the following well, and j_w is the circulating current in the well. For average pulse size $\langle j_p \rangle$, the contribution from the fluctuation in the number of pulses per unit time is

$$S_{jp}^o = \frac{2(j_p)^2 p}{(1 + p\tau)^3} \tag{15}$$

The contribution to S_j^o from the motion within the well can be estimated in the low noise limit by ordinary first order correlation theory following the treatment of Likharev and Semenov for the single junction at $i < i_c$.[23] For a particle confined within the well, the low frequency current noise spectral density is

$$S_\omega^o = \frac{4\Gamma(a^2 + b^2)}{(a + b + \pi\beta ab)^2} \tag{16}$$

where

$$a = (1 - \alpha)\cos_{1\ \min} \tag{17}$$

$$b = (1 + \alpha)\cos_{2\ \min} . \tag{18}$$

We assume that the motion within the well is essentially uncorrelated with the noise generated by the random production of the current pulses.

Thus, for effective pulse rate r and dead time τ,

$$S_j^o \cong S_{jp}^o + (1 - r\tau)\, S_w^o \,. \tag{19}$$

The voltage and current pulses are produced simultaneously, and thus are strongly correlated. Since the voltage noise is dominated by the voltage pulse noise, the low frequency correlation spectral density can be approximated by $S_{vj}^o \sim S_v^o\, S_{Jp}^o$.

Note that Eqs. 11-19 are only valid for bias currents $i \lesssim 1$. At bias current $i \cong 1$ such that $\Delta u \gtrsim \Gamma$, the approximations used to derive Eq. 10 begin to break down. The model seems to work fairly well for values of $\Delta u \gtrsim \Gamma/2$. At bias currents such that $\Delta u < \Gamma/2$, the computed voltage and noise spectral densities decrease rapidly and the model fails. Also note that Eqs. 11-19 have been derived considering motion only in the direction of increasing δ. However, at bias currents $i \cong 0$, the potential difference between successive wells approaches zero. In this case, the particle can make a transition either to the right with probability $p_r = p$ generating a voltage pulse $+2\pi$, or to the left with probability $p_\ell = p \exp(-2\pi i/\Gamma)$ generating a voltage pulse -2π. At $i = 0$, the rates are equal, and $\bar{v} = 0$. Near $i = 0$, $\bar{v}$ is a function of both p_r and p_ℓ. A detailed discussed of this effect can be found in Appendix I.

III. MODEL FOR THE DOUBLE LOOP SQUID MAGNETOMETER

A. Lumped Circuit Element Model

The lumped circuit element model for the double loop SQUID is shown in Figure 9. The superconducting outer loop is divided into two parts by a shorting capacitance C_s with loss R_s. The lower "SQUID" loop of inductance L contains the Josephson junctions. The upper "coupling" loop inductance is L_s. We assume that the current feed is symmetric and the mutual inductance between the loops is negligible. The junction parameters are critical current I_o, shunt resistance R and junction capacitance C. If the device is biased at constant current I, a voltage V appears across the output. The time averaged voltage $\overline{V}$ is then a periodic function of the flux Φ_a threading the superconducting loop.

The equations describing the time development of the junction phase drops, δ_1 and δ_2, are identical to those for the conventional dc SQUID.

$$V_1 = (\Phi_o/2\pi)(d\delta_1/dt) = R(I/2 - J - I_o \sin \delta_2) + V_{N1}, \tag{20}$$

and

$$V_2 = (\Phi_o/2\pi)(d\delta_2/dt) = R(I/2 + J - I_o \sin \delta_2) + V_{N2}. \tag{21}$$

where J is the current circulating in the "SQUID" loop, and V_{N1} and V_{N2} are random voltage noise sources associated with the shunt resistors. The output voltage V satisfies

$$V = (\Phi_o/4\pi)(d\delta_1/dt + d\delta_2/dt). \tag{22}$$

The quantization of the fluxoid through the outer superconducting loop yields

$$(\delta_1 - \delta_2)/2\pi = (L_s K + LJ + \Phi_a)/\Phi_o. \tag{23}$$

where K is the current through the "coupling" loop. The screening currents K and J are related via

$$L_s d^2K/dt^2 + R_s dK/dt + K/C_s = R_s dJ/dt + J/C_s + dV_s/dt \tag{24}$$

Equations 20-24 are the basic equations describing the double junction SQUID. For convenience, we re-express Equations 20-24 in dimensionless units (see Table I). The voltage v across the output is

$$v = \frac{1}{2}\left(\frac{d\delta_1}{d\theta} + \frac{d\delta_2}{d\theta}\right) \tag{25}$$

where

$$\frac{d\delta_1}{d\theta} = \frac{i}{2} - j - \sin\delta_1 + v_{n1}, \tag{26}$$

$$\frac{d\delta_2}{d\theta} = \frac{i}{2} + j - \sin\delta_2 + v_{n2}, \tag{27}$$

$$\delta_1 - \delta_2 = \pi\beta J + \pi\beta_L k + 2\pi\phi_a, \tag{28}$$

and

$$\pi\beta_s\beta_L \frac{d^2k}{d\theta^2} + \beta_s\rho \frac{dk}{d\theta} + k = \beta_s\rho \frac{dj}{d\theta} + j + i_s. \tag{29}$$

Note that the noise current i_s is related to the dimensionless Johnson noise voltage v_s of the loss resistor R_s vis $i_s = \beta_s dv_s/d\theta$.

Equations 25-29 are the basic equations describing the behavior of the double loop magnetometer. Note that these equations reduce to the conventional dc SQUID equations in the limit $\beta_L = 0$. In that case, we have seen that the equations of motion can be derived from a potential $u(\delta_1,\delta_2)$. However, in the general case ($\beta_L \neq 0$), the equations of motion for the double loop SQUID cannot be derived from a potential field. Thus, the thermal activation techniques used to solve the conventional dc SQUID cannot be applied to the double loop structure. However, as we shall see in the next section, there is a range of parameters over which the

TABLE 1

FLUX QUANTUM	Φ_o	1
APPLIED FLUX	Φ_a	ϕ_a
JUNCTION SHUNT RESISTANCE	R	1
JUNCTION CRITICAL CURRENT	I_o	1
BIAS CURRENT	I	i
CIRCULATING CURRENT (SQUID)	J	j
CIRCULATING CURRENT (LOOP)	K	k
OUTPUT VOLTAGE	V	v
NOISE VOLTAGE (SHUNT)	V_{N1}	v_{n1}
	V_{N2}	v_{n2}
NOISE VOLTAGE (LOSS)	V_S	v_s
LOSS RESISTANCE	R_S	ρ
SQUID SCREENING FACTOR	$\beta = 2LI_o/\Phi_o$	
LOOP SCREENING FACTOR	$\beta_L = 2L_S I_o/\Phi_o$	
TOTAL SCREENING FACTOR	$\beta_T = 2L_T I_o/\Phi_o$	
SQUID HYSTERESIS PARAMETER	$\beta_c = 2\pi I_o R^2 C/\Phi_o$	
SHUNTING CAPACITANCE	$\beta_s = 2\pi I_o R^2 C_s/\Phi_o$	
NOISE FACTOR	$\Gamma = 2\pi k_B T/I_o\Phi_o$	
VOLTAGE SPECTRAL DENSITY	$S_V = (S_v/2\Gamma)2k_BTR$	
CURRENT SPECTRAL DENSITY	$S_J = (S_j/2\Gamma)2k_BT/R$	
	$S_K = (S_k/2\Gamma)2k_BT/R$	
CORRELATION SPECTRAL DENSITY	$S_{VJ} = (S_{vj}/2\Gamma)2k_BT$	
	$S_{VK} = (S_{vk}/2\Gamma)2k_BT$	
TRANSFER FUNCTION	$\partial\langle V\rangle/\partial\Phi_a = (\partial\langle V\rangle/\partial\phi_a)I_oR/\Phi_o$	
FLUX NOISE	$S_V/(\partial\langle V\rangle/\partial\Phi_a)^2 = \varepsilon_\phi(2k_BT/I_o^2R)\Phi_o^2$	

conventional and double loop SQUID characteristics are closely related.

B. Double Loop Characteristics Above Tank Circuit Resonance

First, the double loop and conventional dc SQUID equations are identical for all values of the device parameters, provided that the circulating screening current k = j = constant. In that case, the phase drops δ_1 and δ_2 are constant and the double loop SQUID is in the zero voltage state. The screening currents j and k are identical to the screening curent j_T that would flow around a conventional dc SQUID with total loop inductance $L_T = L + L_s$ ($\beta_T = \beta + \beta_s$). Similarly, the dependence of the double loop critical current on the applied flux is identical to the conventional SQUID dependence for a device with screening factor β_T. The conventional dc SQUID dependence of critical current vs. applied flux is plotted in Figure 10 for convenience (from Ref. 14). Note in particular that the modulation depth $\Delta i_c = i_c(\phi = 0) - i_c(\phi = 0.5)$ decreases as β_T increases.

If the double loop SQUID is biased above the critical current in the noise free state, the phase differences and screening currents begin to oscillate in time. For arbitrary initial conditions, a transient will be observed in the screening currents. From Eq. 24, the transient response is given by the resonant frequency and Q of the tank circuit composed of L_s, R_s and C_s in series. The transient response significantly complicates the numerical analysis of the device. A simplification occurs, however, if the resonant frequency of the tank circuit, $\Omega_t = (L_s C_s)^{-\frac{1}{2}}$, lies well below the natural frequency of the junctions, $\Omega_J = (2\pi/\phi_o)\,\bar{V}$ where $\bar{V}$ is the average voltage developed across the device biased at some current $i > i_c$. In this case, the Josephson oscillations of the phase differences δ_1 and δ_2 drive the tank circuit well of resonance. The oscillations in j at the Josephson frequency and harmonies are essentially shorted by the capacitance C_s, and the oscillations in the screening current k can be neglected. In terms of the dimensionless parameters $\beta = 2LI_o/\Phi_o$, $\beta_L = 2L_s I_o/\Phi_o$, $\beta_s = 2\pi I_o R^2 C_s/\Phi_o$, and resistance ratio $\rho = R_s/R$, this corresponds to the condition $\langle v \rangle^2 \pi\beta_L\beta_s \gg 1$. In

addition, we restrict the discussion to a fairly high Q tank circuit, $\beta_s \rho \langle v \rangle \lesssim 1$. This is a physically reasonable assumption, since a low Q tank circuit would introduce excess Johnson noise which would tend to degrade the device performance. The screening current k can now be approximated by the time average, $\langle k \rangle = \langle j \rangle$. Thus, Eq. 28 becomes

$$\delta_1 - \delta_2 = \pi\beta_j + 2\pi (\phi_a + \beta_L \langle j \rangle/2). \tag{30}$$

Equations 25-27 and Eq. 30 correspond to a set of equations isomorphic to the dc SQUID equations with a total applied flux increased by the screening flux $\beta_L \langle j \rangle/2$. Thus, the solution of the conventional dc SQUID equations for screening factor β and applied flux ϕ_T is an approximate solution to the double loop equations with screening factors β and β_L and applied flux ϕ_a if $\phi_a = \phi_T - \beta_L \langle j \rangle/2$. Note that $\langle j \rangle$ is the average circulating current for both the conventional dc SQUID solution and for the double loop solution. Similarly, the average voltage, $\langle v \rangle$, developed across the conventional dc SQUID biased at i and ϕ_T is approximately equal to the average voltage developed across the double loop device biased at i and ϕ_a.

The common solutions can be found using a load line technique. We illustrate the technique for a double loop SQUID with screening factor $\beta = 1$ and $\beta_L = 50$. We plot the average circulating current $\langle j \rangle$ versus applied flux ϕ_T for a conventional dc SQUID with screening factor $\beta = 1$ as a function of bias current in Figure 11. Note that the family of curves are periodic in ϕ_T with period 1 (in dimensioned units, the periodicity is ϕ_o). Only the section $0 \leq \phi_T \leq 1$ has been shown. A load line, $\langle j \rangle = (2/\beta_L)(\phi_T - \phi_a)$, has also been drawn for $\phi_a = 0.25$, $\beta_L = 50$. Note that the load line is not periodic in ϕ_T. As a result, a family of parallel lines appears in the collapsed plot, Figure 11. As the screening factor β_L increases, the slope of the load line decreases, and the separation between the parallel lines decreases. As a result, as β_L increases, the load line will intersect the curve $\langle j \rangle$ vs. ϕ_T for fixed i bias at numerous places. Each point of intersection represents a distinct approximate

solution. The corresponding average voltage, $\langle v \rangle$, can be read off the $\langle v \rangle$ vs. ϕ_T characteristics plotted in Figure 12. In the limit, $\beta_L \to 0$, the load line approaches the vertical. In this case, $\phi_T = \phi_a$ and the conventional dc SQUID and double loop solutions are identical.

Noise free I-V characteristics for a conventional dc SQUID with $\beta = 1$ are plotted for various values of applied flux in Figure 4. All the characteristics are single valued, and lie between the characteristics labled $\phi_T = 0$ and $\phi_T = 0.5$. Noise free I-V characteristics as a function of applied flux for a double loop SQUID with $\beta = 1$ and $\beta_L = 10$ are plotted in Figure 13. Since the average voltage at fixed bias current i for the double loop SQUID corresponds to the conventional dc SQUID voltage at some flux $0 < \phi_T < 0.5$, all the double loop characteristics also lie within the conventional SQUID characteristics labled $\phi_T = 0$ and $\phi_T = 0.5$. In fact, since $\langle j \rangle = 0$ at $\phi_T = 0$ and $\phi_T = 0.5$, the conventional characteristics and the double loop characteristics coincide at those values of applied flux. However, as can be seem from Figure 13, a family of hysteretic solutions also exist. The hysteresis arises because the critical current for the double loop SQUID is identical to the critical current for the conventional SQUID with total screening factor $\beta_T = \beta + \beta_L$. As β_T increases, the critical current $i_c(\phi_a)$ also increases (see Figure 4b). However, as $\langle v \rangle$ increases, the double loop solutions are approximated by conventional solutions for screening factor $\beta = 1$. These characteristics lie below the characteristics for $\beta_T = 11$. As a result, the double loop characteristics droop. In addition, for sufficiently large values of β_L, there are a set of metastable solutions which occur below the critical current. Another set of lobed solutions occur above the critical current (see Figure 14). These solutions correspond to excess flux trapped in the SQUID loop, and cannot be generated from the conventional solutions by smoothly varying the parameter β_L.

Equations 25-29 were also simulated numerically. The equations were integrated stepwise in time using a fourth-order Adams Moulton predictor-corrector method. The instantaneous voltage $v(\theta)$ and circulating currents $j(\theta)$ and $k(\theta)$ were computed at each step interval. The initial conditions were carefully chosen so as to minimize the transient response.

The average voltage was determined by computing the period of oscillation of the phases δ_1 and δ_2. I-V characteristics determined by this method are in excellent agreement with the approximate hysteretic solutions. Appropriate initial conditions could not be determined for the negative resistance region of the hysteretic characteristics, nor for the metastable lobes.

C. Noise Free Characteristics for Arbitrary Parameter Values

Noise free characteristics for arbitrary values of the circuit parameters are generated by direct numerical simulation of the basic equations. In the general case, no simple relationship exists between the double loop characteristics and the conventional dc SQUID characteristics. We are interested in calculating the characteristics for values of the parameters which enhance the coupling properties of the device without degrading the signal-to-noise ratio. A reasonable guess would be to choose values for the resonant coupling circuit consisting of the coupling loop L_s, *shorting capacitance* C_s *and loss* R_s *such that the resonant frequency of* the coupling circit is much less than the Josephson frequency of the junctions, $\omega_t << \omega_J$. As demonstrated in Section III-B, the I-V characteristics in that case become multivalued and show considerable hysteresis. Unfortunately, hysteresis in the I-V characteristics of a conventional dc SQUID near the zero voltage state degrades the performance of the device. To avoid this problem in the double loop SQUID, we must relax the constraint $\omega_t << \omega_J$.

In this section, a family of I-V characteristics is computed for double loop devices with variable resonant frequencies ω_t. If the coupling loop inductance β_L is fixed, the resonant frequency ω_t is a function of the dimensionless shorting capacitance β_s, $\omega_t = (\pi\beta_L\beta_s)^{-\frac{1}{2}}$. We take the resistance ratio $\rho = R_s/R << 1$ to reduce the Johnson noise generated in the loss resistance R_s (the noise free characteristics are essentially independent of ρ in this limit).

The I-V characteristics generated by numerical simulation are plotted in Fig. 15 as a function of ω_t. The screening factors are $\beta = 1.0$, $\beta_L = 10.0$

and the applied flux $\phi_a = 0.25$. For comparison, the dimensionless Josphson frequency $\omega_J = \langle v \cdot$. Thus, the curve labled $\beta_s \simeq 10$, $\omega_t \simeq 0.06$ corresponds to the hysteretic approximate solution for $\omega_t << \omega_J$ found in Section III-B. Note that the negative resistance region and metastable lobes were not generated in the numerical simulation. As ω_t is increased, the hysteresis near the zero voltage state increases. In fact, the characteristic plotted in Fig. 13 for $\omega_t = 0.15$ lies below the conventional dc SQUID characteristic for $\beta = 1$, $\phi_T = 0.5$. In this case, the double loop behavior clearly cannot be approximated by the conventional dc SQUID behavior. However, at bias currents such that $\omega_J = \langle v \cdot \rangle > 0.15$, the characteristic approaches the approximate solution found in Section III-B.

The I-V characteristic for $\omega_t = 0.3$ shows a qualitatively different behavior. In this case, the tank circuit resonant frequency, ω_t, corresponds to the average voltage near the bottom of the droop in the approximate solution. As a result, for $\langle v \rangle \lesssim \omega_t$, the Josephson oscillations are not effectively shorted out by the capacitance C_s. The device behaves like a conventional dc SQUID with $\beta = 11$, $\phi_a = 0.25$. No hysteresis is observed near the zero voltage state. In the region $\langle v \gtrsim \omega_t$, the double loop characteristic begins to deviate from the $\beta = 11$ dc SQUID characteristic. Furthermore, the numerical simulation becomes somewhat unstable. The character of this instability can be seen in Fig. 16. The instantaenous voltage v and screening currents k and j are plotted as a function of time, θ, for a double loop SQUID with $\beta = 1$, $\beta_L = 10$ and $\beta_c = 0.3537$. At bias current $i = 2.0$, ($\omega_J < \omega_t$) the Josephson frequency $\omega_J < \omega_t$, and the voltage and screening currents are periodic functions of time as expected. However, if the bias current is increased to $i = 2.25$, the Josephson frequency approaches the resonant frequency of the coupling loop. At this point, the voltage and circulating currents are no longer periodic functions of time. If the bias current is then increased to $i = 2.4$, $\omega_J > \omega_t$ and the periodic relationships between v, j and k and the time θ return. This kind of behavior is characteristic of chaotic systems. In this case, the equations of motion can be reduced to a set of coupled third order non-linear differential equations describing

a system of two lightly damped non-linear oscillators with nearly equal characteristic frequencies. Chaotic behavior in systems of this nature has been described in detail.[28,29] From a practical standpoint, we expect chaotic behavior to be accompanied by a continuous low frequency voltage power spectral density, even in the absence of Johnson noise sources. Although chaotic behavior in Josephson junction devices is a subject of considerable interest, a careful investigation of this behavior in the double loop device is outside the scope of the present effort.

At bias currents $i \tilde{>} 2.2$, instabilities in the calculation of the I-V characteristic labled $\omega_t = 0.3$ are no longer observed. In this region, a hysteresis loop is observed. Note that both branches of the loop are numerically stable. At bias currents $i > 3.0$, the characteristic approaches the approximate solution for the limit $\omega_t \ll \omega_J$. In this region, both solutions are nearly equal to the conventional dc SQUID solution for $\phi_a = 0.5$, $\beta = 1$.

The final characteristic plotted in Fig. 15 corresponds to the limit $\omega_t \gg \omega_J$, for frequencies ω_J within the hysteretic region in the approximate solutions (i.e., $\omega_t \simeq 0.6$). In this case, the I-V characteristic is nearly identical to the conventional dc SQUID characteristic for $\beta = 11$, $\phi_a = 0.25$. Furthermore, no instabilities in the simulation were observed. This is probably because the non-linearities associated with the Josephson junctions are small in the region $\omega_t \sim \omega_J$. As a result, chaotic effects are less likely.

In conclusion, the only characteristics in Fig. 15 which are non-hysteretic satisfy $\omega_t \tilde{>} 0.6$. In this case, the shorting capacitance is essentially irrelevant, and the characteristics reduce to the conventional dc SQUID characteristic with $\beta_T = \beta + \beta_L$. As ω_t is decreased, the I-V characteristics begin to deviate from the conventional dc SQUID characteristics. In particular, a hysteresis loop is observed at bias currents $i > i_c$. For sufficiently low values of ω_t, the hysteresis occurs near the zero voltage state.

D. Numerical Techniques for Double Loop Characteristics with Noise

In this section, the numerical techniques used to compute device characteristics in the presence of noise are discussed. The dominant noise sources within the device are assumed to be the Johnson noise generated by the junction shunt resistances and the tank circuit resistance, R_s. The effect of low frequency noise sources will not be discussed in this section. We assume that the device parameters and operating point are chosen such that the power spectral density of the voltage noise source associated with each resistance is white at all relevant frequencies. For a device generated at temperature T, the corresponding average voltage across the device must satisfy $V = \langle v \rangle I_o R << 2\pi k_B T/\Phi_o$. The voltage noise sources are uncorrelated, with shunt power spectral density $S_N = 4k_B T R_s$ and loss power spectral density $S_s = 4k_B T R_s$. In dimensionless units, $S_n = 4\Gamma$ and $S_s = 4\Gamma\rho$.

In the conventional dc SQUID, the equations of motion written in dimensionless form are independent of the shunt resistance, R. As a result, the energy factor S_E scales with the shunt resistance, $S_E \propto 1/R$. The value of R is limited by the constraint $\beta_c = 2\pi I_o R^2 C \lesssim 1$. The dimensionless equations of motion for the double loop SQUID are also independent of R. However, the equations are a function of the resistance ratio $\rho = R_s/R$. As we have seen in Section III-C, the noise free I-V characteristics are relatively independent of ρ, provided $\beta_s \rho \langle v \rangle \lesssim 1$. In the noise rounded [illegible], however, any noise generated by the loss resistor will tend to degrade the resolution of the device. Thus, we are interested in computing the characteristics for device parameters such that the noise currents generated by the loss resistance are small compared to the noise currents generated by the junction shunt resistance.

An indication of the relative importance of the noise currents generated in the device is obtained by taking the limit $I_o = 0$. In this limit, the shunted junctions are replaced by the shunt resistances (see Figure 17). The device now consists of ordinary linear circuit elements with uncorrelated white voltage noise sources in series with the resistances R and R_s. The voltage noise source V_s in series with R_s generated a current I_s through the shorting capacitance C_s. This noise source affects the device

in two ways. First, noise components near the Josephson frequency ω_J will contribute to the noise rounding of the I-V characteristics. In addition, the noise will be mixed down by the non-linear interaction in the junctions and appear as a contribution to the low frequency voltage and current noise. In addition, the component of I_s near the tank circuit resonance, ω_t, can link noise flux into the device through the inductances L and L_s. Since the I-V characteristics and device noise spectral densities are a function of the quasistatic applied flux Φ_a, the device characteristics at frequencies $\omega << \omega_t$ can be approximated by a weighted average of the characteristics over the variance in the flux produced by the noise in the loss resistor R_s. If the flux resolution is a sharp function of the applied flux, the average resolution may be reduced considerably.

As an example, consider a double loop SQUID with $\beta = 1$, $\beta_L/\beta = L_s/L >> 1$. Let the resonance frequency of the tank circuit $\omega_t << \omega_{Jo} = 2\pi I_o R/\Phi_o$. The noise current $I_s = V_s/Z_T$ where

$$Z_T = R_s\,[1 + 2\rho\gamma Q^2(\omega/\omega_t)^2] + jR_s\,[\gamma Q(4 + \omega^2 LL_T/R^2)(\omega/\omega_t) - Q(\omega_t/\omega)] \quad (31)$$

and

$$\gamma = (4 + \omega^2 L_T^2/R^2)^{-1} \quad (32)$$

Case A: $\omega_t L_T \cong \omega_t L_s >> 2R$. In dimensionless units, $\rho Q >> 2$. This condition is equivalent to $\beta_L \omega_t/\omega_{Jo} >> 1$. At frequencies $\omega \sim \omega_{Jo}$, $\gamma \cong R^2/\omega^2 L_T^2$, and $Z_T \cong R_s\,(1 + 2/\rho) + jR_s Q/\beta_L$. The fraction of the current noise from R_s flowing around the SQUID loop is $S_{Js} = 4k_B T R_s/|Z_T|^2 \cong 4k_B T/R_s\,[(1 + 2/\rho)^2 + Q^2/\beta_L^2]$. By comparison, the current noise from the shunt resistances flowing in the SQUID loop is $S_{JN} \cong 4k_B T(2R)/R^2[(2 + \rho)^2 + (\pi\omega/\omega_{Jo} - Q\rho\omega_t/\omega)^2]$. Thus the noise from the loss resistor can be neglected if $(2/\rho)[(2 + \rho)^2] >> (2 + \rho)^2 + [\pi(\omega/\omega_{Jo}) - Q\rho\,(\omega_t/\omega)]^2$ (note $\rho Q/\beta_L << 1$). Now $Q\rho(\omega_t/\omega) \cong Q\rho\,(\omega_t/\omega_{Jo}) \cong 2\beta_L(\omega_t/\omega_{Jo})^2$. Thus, we need $\beta_L\,(\omega_t/\omega_{Jo})^2 \rho << 4$, $\rho << 1$. If ρ is small enough to satisfy both of these conditions, the effects of the noise from R_s on the junctions can be neglected. At

frequencies near the resonant frequency, ω_t, $\gamma \sim R^2/\omega_t L_T^2 \sim 1/Q^2\beta^2$, and $Z_T \sim R_s\ (1 + 2/\rho) + jR_sQ$. For $\rho \ll 1$, $S_{Js} \cong 4k_BT/R_sQ^2$. The noise flux spectral density is $S_{\phi s} \cong 4k_BTL^2/R_sQ^2$ over a bandwidth $\Delta f \cong \omega_t/2\pi Q$. The variance $\Delta\phi^2/\phi_o^2 \sim (\Gamma/2\pi)(\omega_t/\omega_{Jo})(1/\rho Q^3) \ll 1$. Thus the noise flux through the SQUID loop can be neglected. The noise current through the coupling loop $S_{Ks} \sim S_{Js}\ (2R/\omega_t L_s)^2$ produces a noise flux of $S_{\phi c} = L_s^2 S_{Ks} \sim (L_s/L)^2(2R/\omega_t L_s)^2\ S_{\phi s}$. The variance $\Delta\phi^2/\phi_o^2 \sim (\Gamma/2\pi)(\omega_{Jo}/\omega_t)(1/\rho Q^3) = (\Gamma/16\pi)(\omega_{Jo}/\omega_t)^4(\omega^2/\beta_L{}^3)$. Since $\beta_L \gg 1$ and $\beta_L(\omega_t/\omega_{Jo}) \gg 1$, this condition also places an upper limit on ρ. Note that the amount of variance in flux at ω_t which can be tolerated without serious loss of resolution depends on the detailed dependence of the energy resolution on applied flux.

Case B: $\omega_t L_T \sim \omega_t L_s \ll 2R$. In dimensionless units $\rho Q \ll 2$ and $\beta_L(\omega_t/\omega_{Jo}) \ll 1$. Near the resonance frequency, $\gamma \sim 0.25$ and $Z_T \cong R_s (1 + \rho^2Q^2/2\rho) + jR_sQ^3\rho^3/4\rho\beta_L$. The flux noise generated through the coupling loop is $S_{\phi c} \sim L_s^2\ S_{vs}/|Z_T|^2 \sim 4k_BTR_sL_s^2/R_s^2(1+\rho Q^2)^2$. Since $\beta_L \gg 1$, the averaging over the characteristics produced by V_s can be large unless $\rho Q^2 \gg 1$. Since $\rho Q \ll 2$, this places a constraint on both ρ and Q, $1/Q^2 \ll \rho \ll 2/Q$ and $Q \gg 1$.

In conclusion, the effect of the noise source V_s on the device characteristics can be ignored for a wide range of device parameters. For a double loop SQUID with resonant frequency $\omega_t \ll \omega_{Jo}$ and coupling loop inductance $L_s \gg L$, the requirement is typically $R_s \ll R$.

We assume that the double loop SQUID parameters are chosen such that the noise in V_s can be ignored. In this case, the device characteristics are computed as follows. Equations 25-29 are integrated stepwise in time on a computer. The noise sources in the shunt resistors, v_{n2} and v_{n2}, are approximated as follows. The Johnson noise terms are considered to consist of a chain of pulses of equal duration $\Delta\theta$ and random amplitude v_k. The amplitudes $\{v_k\}$ should be chosen such that the voltage noise power spectral density is white, with value $S_n(f) = 4\Gamma$ for $\Gamma = 2\pi k_BT/I_o\phi_o$ (in dimensioned units, $S_N(F) = 4k_BTR$).

To facilitate the computation, the noise source is artificially smoothed by taking the Fourier transform of the voltage amplitudes $\tilde{v}_k = a \exp [in_k]$, where n_k is a pseudorandom number uniformly distributed in the range $(0, 2\pi)$. Thus the spectral density $S_n(f) = 2\Gamma$ at all values of f for each individual run. The total number of pulses in a run, N, and the pulse duration, $\Delta\theta$, are chosen such that the minimum frequency component $f_{min} = 1/N\Delta\theta \ll \omega_t$, where ω_t is the tank circuit resonant frequency. In addition, the maximum frequency component must satisfy $f_{max} = 1/2\Delta\theta \gg \omega_J$, where ω_J is the fundamental frequency of the Josephson oscillations. Since we are interested in computing the characteristics for the case $\omega_t \ll \omega_J$, these conditions imply that N must be a large number. Typical values are $f_{min} \lesssim \omega_t/20$, $\omega_t \lesssim \omega_J/10$, and $N \sim 2048$.

The differential equations, Eqs. 11-15, are then integrated stepwise in time using a fourth-order, Adams Moulton Predictor-corrector method. The instantaneous voltage $v(\theta)$ and circulating currents, $j(\theta)$ and $k(\theta)$ are computed at each step interval. Noise rounded i-v characteristics are calculated by computing the average voltage $\langle v \rangle$ over typically 40 sets of 2048 intervals. The initial values for the integration are carefully chosen so that no transient response is apparent in the average voltage. Noise power spectral densities S_v, S_j, S_k, S_{vj} and S_{vk} are determined from the average of the products of the Fast Fourier Transform of the appropriate variables for a single run. We estimate the average voltage to be accurate to about 1% and the noise power spectral densities to be accurate to about 15%

E. NOISE ROUNDED CHARACTERISTICS FOR THE DOUBLE LOOP SQUID

In this section we calculate noise rounded characteristics for two particular devices. First, we consider a double loop SQUID with $\beta = 1$, $\beta_L = 1$ and $\omega_o << \omega_{Jo}$. A device which is similar to this structure is presently under construction by Ho Jung Paik and co-workers. The device has been fabricated in a toroidal geometry with point contacts as the Josephson junctions.[24] In this case, the coupling properties are enhanced by the properties of the toroidal geometry, rather than by an increase in the coupling loop β_L. Next, we consider a double loop SQUID with $\beta = 1$, $\beta_L = 10$. In this device the coupling loop inductance has been increased by an order of magnitude. Significant deviation from the conventional dc SQUID behavior are expected in this case.

1. Double Loop SQUID with $\beta = 1$, $\beta_L = 1$

The device parameters are chosen such that the resonant frequency $\omega_o << \omega_{Jo}$, and the resistance ratio $\rho << 1$. We take $\beta_s = 2\pi I_o R^2 C_s/\Phi_o = 100$ and $\rho = R_s/R = 0.01$. Calculations are performed for a moderately noise rounded device, $\Gamma = 0.01$. The resonant circuit $Q = (1/\rho)(\pi\beta_L/\beta_s)^{\frac{1}{2}} = 18$, and the ratio $(\omega_t/\omega_{Jo}) = 0.056$. Note that $\rho Q \simeq 0.2$ and the device is near the case B limit. In particular, $1/Q^2 \simeq 0.003 < \rho < 2/Q \simeq 0.1$. The ratio (ω_t/ω_{Jo}) and the resonant circuit Q are chosen to facilitate the numerical calculation. Note that the calculation has been performed for a relatively low value of Q. In general, a transient will be generated in the circuit at the beginning of the numerical simulation. The size of the transient is determined by the initial values of the phases and circulating currents. The transient decay time is determined by the Q of the tank circuit. In the case $\omega_t << \omega_{Jo}$, $Q >> 1$, the integration must be carried out for a large number of Josephson periods before useful data is generated. To avoid this problem, we have performed the calculation for a relatively low value of Q. We expect the results to be relatively independent of Q, provided $Q >> 1$, $\rho << 1$ and $\omega_t < \omega_{Jo} << 1$.

A family of characteristics for a double loop SQUID with the parameters listed above is plotted in Figure 18. For comparison, we also plot noise rounded characteristics for a conventional dc SQUID with the same total loop inductance $\beta_T = \beta + \beta_L = 2$. In principle, the input signal can be coupled into the entire superconducting loop. Thus the input inductance of the device is given by β_T, rather than by β_L. As a result, the energy resolution of the double loop SQUID should be compared to the resolution of a conventional dc SQUID with screening factor β_T.

The double loop I-V characteristics are plotted in Figure 18a. The noise free characteristic labled $\Gamma = 0$ is hysteretic, with critical current $i_c = 1.75$. Solutions in the negative resistance region of the characteristic could not be generated numerically. Note that the noise rounded characteristic labled $\Gamma = 0.01$ lies below the noise free curve. In the conventional dc SQUID, the opposite behavior is observed. Also note that the double loop I-V characteristic is not well approximated by the noise rounded dc SQUID characteristic for $\beta_T = 2$.

The forward transfer function, $\partial \langle v \rangle / \partial \phi_a$, is plotted as a function of bias current for $\phi_a = 0.275$ in Figure 18b. At bias currents $i \gtrsim 2.0$, the double loop transfer function for $\Gamma = 0.01$ is identical to the noise free value. The noise free transfer function becomes infinite as the characteristic approaches the negative resistance region ($i \sim 1.7$). The noise rounded characteristic is well behaved in this region. The noise rounded double loop transfer function is not well approximated by the conventional noise rounded SQUID characteristic for $\beta_T = 2$. The low frequency voltage and current noise spectral densities are plotted in Figure 18(c)-(g). Curves are plotted for a double loop SQUID with $\phi_a = 0.25$ and $\phi_a = 0.3$, and for the conventional dc SQUID at $\phi_a = 0.25$. The low frequency voltage noise spectral density S_v^o peaks up near the critical current $i_c \sim 1.75$. At this bias current, the double loop value is more than twice the conventional dc SQUID value for $\beta_T = 2$. At bias currents $i \gg i_c$, the voltage noise spectral densities approach the

spectral density of the parallel shunt resistances, $S_v^o \rightarrow 2\Gamma$. The low frequency current noise spectral densities S_j^o and S_k^o plotted in Fig. 18 (d)-(e) also peak near i_c. However, at this bias current, the conventional $\beta_T = 2$ SQUID and double loop spectral densities are nearly equal. Since the conventional SQUID current noise tends to decrease for increasing screening factor (see Appendix I), the double loop current noise is actually depressed below the conventional value for SQUID $\beta_T = 1$. At bias currents $i \gg i_c$, the current noise spectral densities approach the value for the series combination of the shunt resistances S_j^o, $S_k^o \rightarrow 2\Gamma$. The voltage and current noise spectral densities are strongly correlated near i_c (Fig. 15 (f)-(g)). At bias currents $i \gg i_c$, the noise sources are essentially uncorrelated.

The dimensionless low frequency flux noise $\varepsilon_\phi^o = (S_v^o/2\Gamma)/(\partial\langle v\rangle/\partial\phi_a)^2$, is plotted as a function of bias current in Fig. 18(h). From Table 1, the dimensioned low frequency flux noise $S_\phi^o = \varepsilon_\phi^o (2k_BTR)/(I_oR/\phi_o)^2 = \varepsilon_\phi^o(2k_BT/I_o^2R)\phi_o^2$. This is the equivalent flux noise at the input which would produce the voltage noise observed at the device output. Note that the minimum dimensionless flux noise for the double loop SQUID is almost identical to the minimum for the conventional dc SQUID with the same total loop inductance. Furthermore, since the dimensioned flux noise is a function only of the junction parameters I_o, R and T, and the dimensionless factor ε_ϕ^o, the dimensioned flux noise is also the same in both cases. Thus, although the two devices has dissimilar I-V characteristics, forward transfer functions and voltage spectral densities, the effective input flux noises are the same. Also note that in the conventional SQUID, the minimum flux resolution, the maximum voltage noise spectral density and the maximum forward transfer function all occur at approximately the same values of bias current, $I \sim 1.75\ I_o$. For the double loop SQUID, however, the minimum flux noise occurs at bias current $i \sim 1.9$-2.0. This is the value at which the noise rounded average voltage began to decrease below the noise free values (i.e., the hysteresis in the I-V curve began to affect the device performance). Thus, in operating this device, it is important to choose that value of bias current which optimizes the

flux resolution (i.e., $I = 1.9\ I_o$) and not the value which optimizes the forward transfer function (i.e., $I = 1.7\ I_o$).

The magnetic field resolution of the double loop SQUID is proportional to the energy factor S_E. If the input signal is coupled to the entire superconducting loop inductance L_T, the energy factor is $S_E = S_\phi^o/2L_T$. As we have seen, the flux noise S_ϕ^o for a double loop SQUID with $\beta = 1$, $\beta_L = 1$ is nearly identical to that of a conventional dc SQUID with the same total loop inductance. Thus the energy factor and input inductance of the two devices are almost the same. As a result, the magnetic field resolution of the two devices used directly as sensors will be similar. The main different is that the double loop SQUID structure can be easily realized in a toroidal geometry. Thus if the device is coupled through a mutual inductance to a coupling coil in series with a pick-up loop, the superior coupling properties of the toroidal geometry may be exploited to improve the magnetic field resolution.

2. Double Loop SQUID with $\beta = 1$, $\beta_L = 10$

Results for the double loop SQUID with SQUID loop $\beta = 1$ and coupling loop $\beta_L = 10$ are plotted in Fig. 19 (a)-(h). Calculations are performed for $p = 0.1$ and $\beta_s = 10$. For these values, the resonant circuit $Q = 18$ and the ratio $(\omega_t/\omega_{J0}) = 0.056$ as in the previous case. The total superconducting loop inductance $\beta_T = 11$. The critical current in the noise free case is $i_c = 1.93$ at $\phi_a = 0.25$. As a result, the noise free double loop characteristic plotted in Fig. 19 (a) shows substantial hysteresis. Calculations are performed for a relatively low value of the noise figure, $\Gamma = 0.001$, to illustrate the effects of this hysteresis on the noise rounded characteristics.

The noise rounded I-V characteristic is plotted in Fig. 19 (a). The characteristic is almost identical to the noise free double loop characteristic for $i > 1.9$. Below this value, the noise rounded characteristic switches rapidly to the zero voltage state. At this value of bias current, the double loop noise free characteristic was generated from the conventional dc SQUID characteristic for $\beta = 1$, and effective flux $\phi_e \sim 0.4$. The critical current of a conventional SQUID with $\beta = 1$, $\phi_a = 0.4$, is $i_c = 1.26$. Thus the double loop noise free behavior in the region $i \gtrsim 1.9$ is similar to a conventional SQUID biased well above its critical current. The noise rounding of the I-V characteristics of a conventional dc SQUID is negligible for $\Gamma = 0.001$ in this region.

The similarity between the double loop characteristics for $\phi_a = 0.25$, $i \gtrsim 1.9$ and the conventional dc SQUID characteristics for $\beta = 1$, $\phi_e = 0.4$ is also apparent in the plots of the double loop forward transfer function, $\partial \langle v \rangle / \partial \phi_a$, and voltage noise spectral density $S_v^o/2\Gamma$ (Fig. 19 (b)-(c)). The transfer function for $\Gamma = 0.001$ is nearly identical to the noise free value for $i > 1.9$ as expected for a device biased well above its critical current. The voltage spectral density also rapidly approaches the value for a conventional device biased well above the critical current, $S_v^o \to 2\Gamma$, at bias currents $i \gtrsim 1.9$. For comparison, the voltage noise spectral density of a conventional dc SQUID with $\beta = 11$ is $S_v^o/2\Gamma \sim 70$. This discrepancy between

the behavior of the double loop SQUID with $\beta_T = 11$ and the conventional SQUID with the same loop inductance, $\beta = 11$, is even more striking than in Section III.E.1. Below $i = 1.9$, the voltage noise increased dramatically as the SQUID switches to the zero voltage state, then falls to $S_v^o/2\Gamma < 10^{-2}$.

The low frequency double loop SQUID circulating current noise spectral densities, $S_j^o/2\Gamma$ and $S_k^o/2\Gamma$, are similar (Fig. 19 (d)-(e)). Both values are depressed below the value for the isolated shunt resistances, $S_j^o = 2\Gamma$, at $1.9 \lesssim i \leq 2.1$. As the SQUID switches to the zero voltage state, the current noises increase slightly. However, the increase is significantly less than that observed for the voltage noise, because the device is switching between states of similar circulating current. The low frequency noise in the current j and k are moderately correlated with the voltage noise (Fig. 19 (f)-(g)).

The double loop SQUID flux noise spectral density, $\varepsilon_\phi = (S_v^o/2\Gamma)/(\partial v/\partial \phi_a)^2$ is plotted as a function of bias current for $\phi_a = 0.275$ in Fig. 19 (h). Above $i = 1.9$, the flux noise is well approximated by the conventional dc SQUID value for a SQUID with $\beta = 1$, $\phi_a = 0.4$. The flux noise for this device reaches a minimum near $i_c = 1.26$. However, the double loop flux noise increases rapidly at $i < 1.9$ due to the hysteresis in the I-V characteristic. As a result, the minimun double loop flux resolution, $\varepsilon_\phi^{min.} \sim 90$, is similar to the minimum value for a conventional dc SQUID with $\beta = 11$, $\phi_a = 0.25$, $\varepsilon_\phi^{min.} \sim 100$. Thus, although the device characteristics are similar to a conventional SQUID with $\beta = 1$, $\phi_a = 0.4$ for $i > 1.9$, the minimum flux resolution is limited to a value determined by the total loop inductance $\beta_T = 11$.

IV. ANALYSIS OF CONVENTIONAL DC SQUID MAGNETOMETER SYSTEMS

In this section a model is developed for conventional dc SQUID magnetometer systems. Two examples are given. First, the dc SQUID is coupled inductively to a superconducting input circuit containing a pick-up coil and an input coil in series. Next, the effect of including a resistance in series with the input inductance is investigated. This calculation is a generalization of the model for the dc SQUID magnetometer described by Clarke, Tesche and Giffard (CTG).[25]

A. DC SQUID with Superconducting Input Circuit

A conventional dc SQUID coupled inductively to a superconducting input circuit is shown in Fig. 20 (a). The external quasistatic flux ϕ_a is applied to a pick-up inductance L_p in series with an input inductance L_i. The mutual inductance between the input inductance and the SQUID loop is $M^2 = \alpha^2 L L_i$. The effects of stray capacitance within the input circuit and between the input circuit and the SQUID loop are not included in this model.

Flux is quantized in the input circuit. As a result, the circulating current, J, in the SQUID loop generates a superconducting screening current, H, in the input circuit satisfying

$$(L_i + L_p)\, H + MJ + \phi_a = 0. \tag{33}$$

Quantization of the fluxoid in the SQUID loop implies

$$D = LJ + MH \tag{34}$$

where $D = (\Phi_o/2\pi)(\delta_1 - \delta_2)$. Combining Eqn. 33 and 34,

$$D = L_e J + \phi_e, \tag{35}$$

where

$$L_e = L(1 - \alpha^2 r) \tag{36}$$

$$\phi_e = \alpha r (L/L_i)^{\frac{1}{2}} \phi_a \qquad (37)$$

and

$$r = L_i/(L_i + L_p). \qquad (38)$$

Eqn. 35 is the analog of the fluxoid quantization condition for an isolated dc SQUID. The equations of motion for the phase drops δ_1 and δ_2 are the usual junction relations, Eqn. 26 and 27. The voltage across the SQUID output satisfies Eqn. 25. As a result, the equations for the superconducting dc SQUID magnetometer are identical to those of an isolated dc SQUID with loop inductance L_e and applied flux Φ_e.[14]

The superconducting dc SQUID magnetometer may be modeled as a conventional dc SQUID with input inductance L_p. The device forward transfer function $(\partial\bar{V}/\partial\Phi_a) = (\partial\bar{V}/\partial\Phi_e)(\partial\Phi_e/\partial\Phi_a)$, where $(\partial\bar{V}/\partial\Phi_e)$ is evaluated for a dc SQUID with loop inductance L_e biased at applied flux Φ_e. Similarly, the voltage noise spectral density is S_v, and the current noise spectral density through the inductance L_p is $S_H = M^2 S_J/(L_i + L_p)^2$, where S_v and S_J are evaluated for loop inductance L_e and applied flux Φ_e. The correlation factor for the equivalent SQUID, $C_p^2 = (S_v S_J - S_{vJ}^2)/S_{vJ}^2$ is identical to the correlation factor for the isolated SQUID with inductance L_p and applied flux Φ_e.

B. DC SQUID with Lossy Input Circuit

A magnetometer system consisting of a dc SQUID coupled inductively to an input circuit containing a resistive element is shown in Fig. 20(b). A normal resistance R_i is in series with the pick-up coil inductance L_p and coupling coil inductance L_i. The effects of stray capacitance within the input circuit and between the input circuit and the SQUID are not included in the analysis. The introduction of loss into the input citcuit destroys the quantization of flux within that loop. As a result, the behavior of the lossy magnetometer differs significantly from the behvaior of magnetometers with superconducting input circuits.

The equations of motion for the system are as follows. The equations describing the development of the junction phase drops (Eqn. 26-27) and the expression for the voltage across the SQUID (Eqn. 25) are identical to the isolated SQUID equations. The equation describing fluxoid quantization in the SQUID loop is similar to the superconducting magnetometer relationship,

$$D = LJ + MH + \Phi_B \tag{39}$$

Note that we have introduced a bias flux Φ_B into the SQUID loop. In the isolated SQUID operated in a flux locked loop, the bias flux usually consists of both dc and ac components. The analog of Eqn. 33 is given by the voltage drop around the input circuit,

$$(L_i+L_p)\, dH/dt + MdJ/dt + R_iH + d\Phi_a/dt + V_{NI} = 0 \tag{40}$$

where V_{NI} is a random voltage generated by the Johnson noise in the resistor R_i. Eliminating the input circuit current H between Eqn. 39 and Eqn. 40 yields

$$\frac{d(D-L_eJ)}{dt} = -\frac{(D-LJ)}{\tau} + \frac{\Phi_B}{\tau} + \frac{d\Phi_B}{dt} - \frac{M}{(L_i+L_p)}\left(\frac{d\Phi_a}{dt} + V_{NI}\right), \tag{41}$$

where $\tau = (L_i + L_p)/R_i$ and the screened inductance is L_e (Eqn. 36). Thus the equations determining the output voltage V as a function of the applied flux Φ_a are Eqn. 26, Eqn. 27 and Eqn. 41.

The basic equations for the lossy magnetometer are independent of the dc value of the externally applied flux Φ_a. As a result, the system cannot be described by an equivalent device with forward transfer function $\partial\bar{V}/\partial\Phi_a$. Instead, we shall compute the response of the system to a time dependent applied flux $\Phi_a(t)$.

As an example of the technique to be used, consider the following case. Let the input circuit parameters and coupling efficiency be such that the screened loop inductance $L_e \approx L$ ($\alpha^2 << 1$). Consider the noise free case, $V_{NI} = 0$, with bias flux $d\Phi_B/dt = 0$. Eqn. 41 reduces to

$$\frac{d}{dt}(D-LJ) = -\frac{(D-LJ)}{\tau} + F(t) + \Phi_B/\tau \tag{42}$$

where $F(t) = -M(d\Phi_a/dt)/(L_i + L_p)$. This expression can be integrated for a single Fourier component of F(t) of the form $F_n \sin \omega_n t$

$$D - JL = C \exp(-t/\tau) + A_n \sin(\omega_n t - \theta_n) + \Phi_B \tag{43}$$

where

$$A_n = \tau(1+\omega^2\tau^2)^{-\frac{1}{2}} F_n \tag{44}$$

and

$$\theta_n = \tan^{-1}(\omega\tau). \tag{45}$$

The constant C is determined by the initial conditions. Note that a sudden change in the dc bias flux Φ_B introduces a transient with $C = \Delta\Phi_B$. A sudden change in the amplitude of the ac applied flux at time t_o introduces a

transient with $C = \Delta A_n \sin(\omega_n t_o - \psi)$.

Eqn. 43 is the analog of the fluxoid quantization expression for the isolated dc SQUID given by Eqn. 28. The form of the two equations are similar. The lossy input circuit has the effect of introducing a transient response time into the quantization condition. A sudden change, $\Delta\Phi_B$, in the dc bias flux through the SQUID loop introduces a transient $\Delta\Phi \exp(-t/\tau)$. In addition, an ac flux, Φ_a, applied to the pick-up coil is equivalent to an ac flux through the isolated SQUID loop with an amplitude and phase shift determined by the input circuit parameters, signal frequency ω, and response time τ.

The well known solutions for the isolated dc SQUID may now be exploited to determine the effective ac forward transfer function and the flux resolution of the lossy magnetometer system. Suppose that the applied flux is oscillating sinusoidally at frequency $\omega \ll \omega_J$. We use a quasistatic approximation to determine the amplitude of the output voltage, V_o, at the signal frequency ω in terms of the amplitude of the applied flux Φ_{ao} and the isolated SQUID forward transfer function, $\partial\bar{V}/\partial\Phi_a$,

$$V_o = \frac{\omega M(\partial\bar{V}/\partial\Phi_a)\,\Phi_{ao}}{R_i\,(1+\omega^2\tau^2)^{\frac{1}{2}}} \tag{46}$$

At frequencies $\omega \ll 1/\tau$, the output signal is reduced. The resolution is determined by comparing the flux noise to the effective signal flux in the isolated SQUID. The mean squared flux noise in bandwidth B is $\Delta\Phi_N = S_\Phi B$, where S_Φ is evaluated at the SQUID bias flux Φ_B (small signal limit). The mean squared signal flux $\Delta\Phi_s$ through the isolated SQUID is related to the mean squared applied flux $\Delta\Phi_a$ via

$$\Delta\Phi_s = \frac{\alpha^2 L_i L}{(L_i+L_p)^2}\,\frac{\omega^2\tau^2}{(1+\omega^2\tau^2)}\,\Delta\Phi_a. \tag{47}$$

The minimum observable applied flux with 1:1 signal-to-noise ratio ($\Delta\Phi_s = \Delta\Phi_N$) is optimized for input circuit parameters $L_i^{opt} = L_p$. In that case

$$\Delta\Phi_a = \frac{(1+\omega^2\tau^2)}{\omega^2\tau^2}\,\frac{4L_p}{\alpha^2 L}\,S_\Phi B. \tag{48}$$

Note that the flux resolution deteriorates at frequencies $\omega \ll 1/\tau$ like $1/\omega^2\tau^2$.

For comparison, the minimum mean square signal flux derived from the CTG model for an input coil in the limit $R_i = 0$, $\alpha^2 \ll 1$ is

$$\Delta\Phi_a = \frac{4L_p S_\phi B}{\alpha^2 L} \tag{49}$$

The optimal input inductance in this limit is $L_i^{opt} = L_p$. Thus the CTG model adequately describes the behavior of the lossy magnetometer in the weak coupling limit at signal frequencies $\omega \gg 1/\tau$.

Equation 48 was derived in the weak coupling limit for the case $V_{NI} = 0$. This approximation is valid provided that the noise rounding of the magnetometer system characteristics are dominated by the Johnson noise sources associated with the shunt resistances in the SQUID rather than by the Johnson noise in the input circuit resistance. We estimate the relative importance of the two noise sources as follows. The input noise appears in Eqn. 41 as a random forcing function $F = -MV_{NI}/(L_i + L_p)$. Since Eqn. 41 is linear, F may be decomposed into a Fourier series and the components integrated following the method used for the applied flux. The spectral density of the resultant flux noise in the integrated equation is

$$S_{\phi I} = \frac{M^2 S_{VI}}{R_i(1+\omega^2\tau^2)} \tag{50}$$

where S_{VI} is the voltage power spectral density of the Johnson noise generated by the input resistance. For comparison, the independent Johnson noise sources associated with the junction shunts may be transformed into an equivalent bias current noise source and an independent flux noise source.[26] The spectral density of the intrinsic flux noise source is

$$S_{\phi s} = \frac{L^2 S_{NI}}{2R^2} \tag{51}$$

where S_{NI} is the voltage power spectral density of the Johnson noise in a shunt of resistance R. We limit the discussion to system parameters such

that $\omega_J \gg 1/\tau$. In this case, the shunt flux noise dominates the input equivalent flux noise at frequencies $\omega \ll \omega_J$ in the optimized system, if

$$S_{VI} \ll (2/\alpha^2)(L_p/L)(\omega L/R)^2 \, S_{NI} \tag{52}$$

In the thermal limit, this constraint is equivalent to the condition $R_i T_i / L_p \ll RT/L$, where the input and shunt temperatures are T_i and T, and $W_J L/R \gtrsim 1$. In this limit, the SQUID characteristics determined by the total noise spectral density near the Josephson frequency are independent of V_{NI}, and the input Johnson noise source may be approximated as a low frequency (quasi-static) noise source.

V. ANALYSIS OF DOUBLE LOOP MAGNETOMETER RESOLUTION

In this section we compute the magnetic field resolution of double loop magnetometer systems. The double loop SQUID may be used directly as a magnetometer, or coupled to an input circuit. In this first case, the flux resolution of the device in the limit $\omega << \omega_J$ is approximately equal to that of a conventional SQUID with the same total loop inductance. The double loop configuration is useful in those cases where a shorting capacitance across the SQUID loop is unavoidable. An example is a thin film gradiometer in the form of a figure eight with both junctions located in one of the loops. In the second case, the magnetometer resolution depends on both the SQUID and input circuit parameters. As an example, we discuss the resolution of a double loop SQUID coupled inductively to a superconducting and normal input circuit in detail.

A. Double Loop SQUID with Superconducting Input Circuit

The magnetic field resolution of the double loop SQUID can be enhanced by coupling the device to a superconducting input circuit (Fig. 21 (a)). The circulating currents in the SQUID oscillating at the Josephson frequency and its harmonics generate flux in the input circuit. Screening currents in the input circuit act back on the SQUID, altering the behavior of the device. As a result, the noise spectral densities and forward transfer function of the device are a function of theinput circuit parameters.

It is useful to model the double loop SQUID plus input circuit as a single superconducting magnetometer with forward transfer function and noise spectral densities referred to the pick-up coil inductance, L_p (See Fig. 21 (a)). The equivalent magnetometer can then be used to replace a conventional dc SQUID in magnetometer and linear amplifier applications (see Ref. 25). The pick-up coil inductance L_p corresponds to the conventional SQUID loop inductance L. The forward transfer function is $\partial\bar{V}/\partial\Phi_a$, where Φ_a is the external flux applied to the pick-up coil. The flux noise $S_\Phi = S_V/(\partial\bar{V}/\partial\Phi_a)^2$, and the noise current S_H through L_p correspond to the conventional flux noise and circulating current noise through the SQUID loop inductance L.

The equations describing the double loop SQUID plus input circuit for the superconducting input circuit (Fig. 21(a)) are as follows. The total flux applied to the input circuit is the external quasistatic flux Φ_a plus the induced flux, MK, generated by the double loop SQUID, where $M^2 = \alpha^2 L_s L_i$. For convenience, we shall assume that the nutual inductance between L_i and L is negligible. Since flux is quantized in the input circuit, the screening current H satisfies

$$H(L_i + L_p) + KM + \Phi_a = n\Phi_o \tag{53}$$

In addition, the fluxoid quantization condition (Eqn. 23) in the SQUID becomes

$$D = LJ + L_s K + MH \tag{54}$$

Thus, Eqn. 23 is replaced by

$$D = LJ + L_e K - \Phi_e \tag{55}$$

where

$$r = L_i/(L_i + L_p), \tag{56}$$

$$\Phi_e = \alpha r \, (L_s/L_i)^{\frac{1}{2}} \, \Phi_a \tag{57}$$

and

$$L_e = L_s \, (1 - \alpha^2 r) \tag{58}$$

The equations describing the development of the phase drops δ_1 and δ_2 (Eqn. 20-22) are unchanged. Eqn. 24 becomes

$$L_e \frac{d^2K}{dt^2} + R_s \frac{dk}{dt} + \frac{k}{C_s} = R_s \frac{dJ}{dt} + \frac{J}{C_s} + \frac{dV_s}{dt} \tag{59}$$

Thus, the basic equations for the double loop SQUID plus input circuit, Eqns. 20-22, are identical to the original equations with effective coupling loop inductance $L_e = L_s\ (1 - \alpha^2 r)$ and applied flux Φ_e.

The forward transfer function which relates the change in output voltage $\Delta\bar{V}$ to the change in externally applied flux $\Delta\Phi_a$ is $\partial\bar{V}/\partial\Phi_a = (\partial\bar{V}/\partial\Phi_e)(\partial\Phi_e/\partial\Phi_a)$ and the voltage noise at the output is S_v^o, where $\bar{V}$ and S_v are computed for a double loop coupling inductance L_e and applied flux Φ_e. The effective flux noise through the pick-up coil is $S_{\Phi p} = S_{\Phi E}\ L_i/\alpha^2 r^2 L_s$. For an effective total inductance $\beta_e \gtrsim 1$, $\Phi_e \sim \Phi_o/4$,

$$S_{\Phi p} \sim 4k_B T\ (L + L_s(1 - \alpha^2 r)]^2\ L_i/\alpha^2 r^2 L_s R.$$

The double loop magnetometer plus input coil can now be represented by an idealized magnetometer with input coil inductance L_p and effective flux noise $S_\Phi p$.

The flux noise, $S_{\Phi p}$, is minimized in the perfect coupling limit, $\alpha^2 = 1$. In that case,

$$S_{\Phi p} \sim (4k_B T/R)\ [LL_i + LL_p + L_s L_p]^2/L_i L_s. \tag{60}$$

The flux noise is minimized for fixed L_p as a function of L_i as follows:

$$L_i^{opt} = L_p\ (1 + L_s/L) \tag{61}$$

$$S_{\Phi e}^{opt} \cong (16\ k_B T/R)(1 + L/L_s)LL_p. \tag{62}$$

We are interested in the limit $L_s \gg L$. In that case, $L_e^{opt} = LL_s/(L_s + 2L) \sim L$ and $L_i^{opt} = L_p(L_s/L)$. The optimal flux noise in this case is limited by the SQUID loop inductance L and input pick-up coil inductance L_p. The inductance L is constrained by $\beta_T \sim 2_p \geq 1$. (Note that the case $\beta = \beta_E = 1$ has been solved numerically in Section III.D.)

The current noise power spectral density through the pick-up coil is

$S_H = M^2 S_{KE}/(L_i + L_p)^2$, where S_{KE} is the current noise power spectral density for a double loop SQUID with screening loop inductance L_e and applied flux Φ_e. In the limit $L_s \gg L$, $\alpha^2 = 1$, $S_H \simeq S_{KE}/(LS_{KE}/L_p)$. The correlation factor for the conventional SQUID is $C_F^2 = (S_V S_J - S_{VJ}^2)/S_{VJ}^2$. Note that the correlation factor for the current H and the output voltage V in the double loop input circuit combination is identical to the correlation factor for the current K and V of the equivalent double loop SQUID. Furthermore, the correlation factor for the double loop SQUID with $\beta = 1$, $\beta_L = 1$ is comparable to the correlation factor of a conventional dc SQUID with $\beta_T = 2$.

It is instructive to compute the energy factor referred to the pick-up coil, $S_{ep} = S_{\Phi E}/2L_p$. In the limit $L_s \gg L$, $S_{EP} \simeq 4k_B T(2L)/R$. The energy factor of a conventional dc SQUID with loop inductance L_T is $S_E \simeq 4k_B T/R$. This is a reassuring result. The noise temperature T_N of a conventional SQUID linear amplifier with a tuned input circuit operated at frequency ω is proportional to the energy and correlation factors, $T_N \simeq \omega C_F S_E/KB$.[25] The optimal source resistance scales with the input SQUID loop inductance L. If we replace the conventional SQUID in the linear amplifier circuit with the double loop plus input circuit combination, the energy factor is unchanged for $L_T = 2L$. In addition, the correlation between the output voltage and the current noise in the pick-up coil is similar tot he correlation between the SQUID output voltage noise and SQUID loop circulating current noise. As a result, the optimal noise temperatures of the two devices are similar. This is important because the noise temperature of a high gain linear amplifier is limited by the uncertainty principle to $T_N \geq \hbar\omega/k_B \ln^2$. This limit is approached for values of the device parameters such that $\hbar\omega_J \gg k_B T$. In this case, the thermal noise sources in the shunted junctions are dominated by quantum fluctuation effects in the SQUID. Minimum noise temperatures computed as a function of the conventional dc SQUID parameters are consistent with the uncertainty principle requirement.[5] Since the behavior of the conventional dc SQUID and the optimized double loop SQUID plus input circuit with $L_T = 2L$ are similar, we expect a detailed analysis would also yield $S_{Ep} \simeq \hbar$, $C_{FE} \simeq C_F$ in agreement with the uncertainty principle limit. However, the optimal source resistance of the

double loop amplifier now scales with the pick-up inductance L_p. This value is not limited by the uncertainty principle.

The procedure for optimizing the magnetic field resolution is the following. The flux noise $S_{\Phi E}$ for the double loop magnetometer can be reduced by lowering the junction loop inductance L. The coupling inductance is increased to $L_s \gg L$ to improve the coupling properties of the double loop SQUID. The inductance L_s is then screened by the superconducting input circuit. The actual input inductance for the combined system is $L_p = (L_i/L_s)L$, where L_i is the largest coil that can be efficiently coupled to the inductance L_s. The inductance screening technique is only advantageous in the limit $\alpha^2 \approx 1$. For $\alpha^2 \neq 1$, $L_s \gg L$, the effective inductance $L_e \approx [L + 2L_s(1 - \alpha^2)]/(2 - \alpha^2)$. If the effective inductance is dominated by L_s rather than by L, the effective flux noise deteriorates like $(L_s/\alpha^2 L)$. This places a limit on the values of L, L_s and L_i, and determines the value of L_p. The magnetic field resolution is then a function of the geometry of L_p, and S_{EP}.

One of the properties of the double loop SQUID is that it permits the use of SQUID geometries with improved coupling properties. For example, a thin film planar double loop SQUID has been fabricated by Jaycox and Ketchen.[27] In addition, a toroidal point contact SQUID similar to a double loop SQUID has been fabricated by Paik.[24] In both cases, the coupling properties of these devices are superior to the conventional planar and cylindrical dc SQUIDs. As a result, the double loop SQUID is a more promising device for the investigation of inductance screening effects. Note, however, that the analysis has ignored any stray capacitance in the circuit. The effects of such a capacitance must be negligible even at the effective Josephson frequency.

B. Double Loop SQJID with Lossy Input Circuit

The analysis of the lossy double loop magnetometer follows the analysis of the lossy dc SQUID system closely. The double loop SQUID is coupled inductively to the input circuit as shown in Fig. 21(b). The mutual inductance between the input and SQUID coupling loop is $M^2 = \alpha^2 L_i L_s$. The mutual inductance between the input circuit and the SQUID loop inductance, L, is taken to be negligible, as is the effect of any stray capacitance in the circuit. The pick-up coil inductance is L_p and the loss is R_i.

The voltage drop around the input circuit is

$$(L_i + L_p)\frac{dH}{dt} + M\frac{dK}{dt} + R_i H + \frac{d\Phi_a}{dt} + V_{NI} = 0, \tag{63}$$

where the flux Φ_a is applied to the pick-up inductance L_p, H is the current flowing in the input coil, and the Johnson noise in the loss R_i is V_{NI}. Quantization of the fluxoid in the SQUID yields

$$D = LJ + L_s K + MH + \Phi_B, \tag{64}$$

where the bias flux to the SQUID loop is Φ_B. Eliminating the circulating current H in the input circuit,

$$\frac{d}{dt}(D - L_e K - LJ) = -\frac{(D - L_s K - LJ)}{\tau_i} + \frac{\Phi_B}{\tau_i} + \frac{d\Phi_B}{dt} - \frac{M}{(L_i + L_p)}\left(\frac{d\Phi_a}{dt} + V_{NI}\right), \tag{65}$$

where $\tau_i = (L_i + L_p)/R_i$ as before, and the screened coupling loop inductance $L_e = L_s(1 - \alpha^2 r)$ for $r = L_i(L_p + L_i)^{-1}$. The voltage drop around the coupling loop in the SQUID yields the analog of Equation 24,

$$L_s \frac{d^2K}{dt^2} + R_s \frac{dK}{dt} + \frac{K}{C_s} + M \frac{d^2H}{dt^2} = R_s \frac{dJ}{dt} + \frac{J}{C_s} + \frac{dV_s}{dt} . \quad (66)$$

The junction equations, Eqn. 20-21, and the output voltage relationship, Eqn. 22, are unchanged.

Following the analysis for the conventional lossy magnetometer, we consider the weak coupling limit ($\alpha^2 \ll 1$, $L_e \approx L_s$). In this case Eqn. 65 has the form

$$\frac{d}{dt}(D - L_s K - LJ) = -\frac{(D - L_s K - LJ)}{\tau_i} + F(t), \quad (67)$$

where the forcing function $F(t)$ is a function of the input and applied flux, and the input Johnson noise voltage. Integrating Eqn. 67 for a single Fourier component of $F(t)$ of the form $F_n \sin \omega_n t$,

$$D - L_s K - LJ = C \exp(-t/\tau_i) + A_n \sin(\omega_n t - \theta_n), \quad (68)$$

where $$A_n = \tau_i (1 + \omega_n^2 \tau_i^2)^{-1/2} F_n, \quad (69)$$

and $$\theta_n = \tan^{-1}(\omega_n \tau_i). \quad (70)$$

Combining Eqn. 68 and Eqn. 66 for constant bias flux Φ_B,

$$M \frac{d^2H}{dt^2} = \frac{C}{\tau_i^2} \exp(-t/\tau_i) - \omega_n^2 A_n \sin(\omega_n t - \theta_n). \quad (71)$$

Eqn. 71 can be used to eliminate the current in the input coil, H, from Eqn. 66 . For times $t \gg \tau_i$, the transient response can be neglected. We express Eqn. 66 in terms of an effective circulating current K_e,

$$L_s \frac{d^2K_e}{dt^2} + R_s \frac{dK_e}{dt} + \frac{K_e}{C_s} = R_s \frac{dJ}{dt} + \frac{J}{C_s} + \frac{dV_s}{dt} , \quad (72)$$

where $$K_e = K - K_o \sin(\omega_n - \theta_n'), \tag{73}$$

$$K_o = \omega_n^2 C_s A_n [(1 - \omega_n^2 L_s C_s)^2 + (\omega_n R_s C_s)^2]^{-\frac{1}{2}} \tag{74}$$

and $$\theta_n' = \theta_n + \tan^{-1} [\omega_n R_s C_s (1 - \omega_n^2 L_s C_s)^{-1}]. \tag{75}$$

In the low frequency limit, $\omega_n^2 << 1/L_s C_s$, $\omega_n << 1/R_s C_s$, $\theta_n' = \theta_n$ and $K_e = K - \omega_n^2 C_s A_n \sin(\omega_n t - \theta_n)$.

The fluxoid quantization condition, Eqn. 68 , can also be expressed as a function of the effective circulating current K_e for times $t >> \tau_i$,

$$D = L_s K_e + LJ + \Phi_e, \tag{76}$$

where the effective flux

$$\Phi_e = A_n \sin(\omega_n t - \vartheta_n) + L_s K_o \sin(\omega_n t - \theta_n'). \tag{77}$$

Eqn. 76 and Eqn. 77 now have the same form as the corresponding equations for the isolated double loop SQUID. As a result, the complete set of equations for the lossy double loop magnetometer, Eqns. 20, 21, 22, 76 , and 77 , can be solved using the same techniques for the isolated driven double loop SQUID. For example, consider a lossy double loop magnetometer system with parameters satisfying $\Omega_J \tau_i >> \Omega_t \tau_i >> 1$ and $R_s C_s \Omega_r << 1$ (see Sec. III B). The effective flux noise components of Φ_e generated by the input resistance at frequencies $\omega_n \geq \Omega_t$ will produce noise rounding of the double loop SQUID characteristics. In this limit, $\theta_n' = \vartheta_n$. The effective flux noise spectral density near resonance is $S_{\Phi I} \simeq L_s^2 S_{VI}/R_s^2$, where S_{VI} is the voltage power spectral density of the Johnson noise generated by the loss R_i. The input and SQUID parameters must be chosen such

that the smearing of the characteristics produced by $S_{\Phi I}$ is negligible (see Sec. III.D). This places an upper limit on the input resistance R_i and temperature T_i.

The effective flux noise at frequencies $\omega_n \simeq \Omega_J$ is $S_{\Phi I} \simeq 4S_{VI}/\omega_n^2$. The equivalent flux noise generated within the SQUID is $S_{\Phi S} = L^2 S_{NI}/2R^2$, where S_{NI} is the voltage spectral density of the Johnson noise generated by the junction shunt (see Sec. IV.B). Thus, the noise rounding of the device characteristics can be neglected provided

$$S_{VI} \ll 8\,(\Omega_J\, L/R)^2\, S_{NI}\,, \tag{78}$$

where the factor $(\Omega_J\, L/R) \simeq 1$ for SQUID loop $\beta = 1$. Note that if the input noise cannot be neglected, the resultant equations cannot be well approximated by those of an isolated symmetric double loop SQUID.

We assume that the effects of the input Johnson noise can be neglected. In that case, for signal frequency $\omega_s \ll \Omega_t$, the applied flux Φ_a through the magnetometer system may be approximated by a *quasistatic effective flux* Φ_e *through an isolated double loop SQUID* (see Sec. IV.B). In this limit, the contribution of the screening current, $K - K_e$, to the effective applied flux can be neglected. As a result, the analysis of the resolution follows the pattern of the conventional lossy dc SQUID magnetometer (Sect. IV.B). The amplitude of the output voltage generated by an applied flux $\Phi_a = \Phi_{ao} \sin \omega_s t$ is

$$V_o = \frac{\omega_s\, M(\partial \bar{V}/\partial \Phi_a)\, \Phi_{ao}}{R_i(1 + \omega_s^2\, \tau_i^2)^{1/2}}\, \sin(\omega_s t - \theta), \tag{79}$$

where $\theta = \tan^{-1}(\omega_s\, \tau_i)$, and $(\partial \bar{V}/\partial \Phi_a)$ is the quasistatic foreward transfer function for the isolated double loop SQUID. The minimum observable mean-squared flux $\Delta\Phi_a$ in bandwidth B for unity signal-to-noise ratio is

$$\Delta\Phi_a = \frac{(1 + \omega_s^2\, \tau_i^2)}{\omega_s^2\, \tau_i^2}\, \frac{4L_p\, S_\Phi\, B}{\alpha^2\, L_s}$$

for optimal input inductance $L_i^{op+} = L_D$. In this expression, S_ϕ is the flux noise spectral density of the isolated double loop SQUID.

VI. SUMMARY

An analysis of double loop SQUID magnetometer systems has been performed. The device consists of a conventional dc SQUID with loop inductance in series with a resonant coupling circuit. A lumped circuit element model for the device has been developed. The equations of motion for the device in the noise free case are seen to be closely related to the conventional dc SQUID equations for devices with coupling loop resonant frequency well below the intrinsic Josephson frequency. The I-V characteristics are found to be hysteretic, with critical current determined by the total loop inductance. In addition, possibly chaotic behavior is observed for devices with resonant frequency on the order of the Jospehson frequency.

Noise rounded characteristics were generated by direct numerical simulation. Optimal flux resolution is obtained at bias currents on the order of the total loop critical current. The device characteristics at that point are well approximated by conventional dc SQUID characteristics for a device with loop inductance equal to the double loop SQUID junction loop inductance. However, the hysteresis in the double loop characteristics limits the minimum flux resolution to a value which is well approximated by the resolution of a conventional device with the same total loop inductance.

The main advantage of the double loop SQUID appears to lie in the enhanced coupling properties which the double loop geometry permits. With that in mind, a model for SQUID magnetometer systems which explicitly includes the effects of the input circuit on the SQUID characteristics was developed. The model was used to calculate the resolution of superconducting and lossy magnetometer system. Inductance screening effects obtainable for input circuits coupled inductively to the SQUID were found to enhance the magnetic field resolution in the good coupling limit. Deterioration of the flux resolution of lossy systems was observed at signal frequencies below the inverse of the input circuit decay time. The effects of stray capacitance within the input circuit and between the input circuit and the SQUID were not considered in this effort. These effects could be substantial if resonant behavior in the input circuit is observed at the coupling loop resonant frequency or at the Josephson frequency.

VII. REFERENCES

1. R.C. Jaklevic, J. Lambe, A.H. Silver and J.E. Mercereau, Phys. Rev. Lett. 12, 159 (1964); Phys. Rev. Lett. 14, 887 (1965); Phys. Rev. 140, A1628 (1965).

2. B.D. Josephson, Phys. Lett. 1, 251 (1962); Adv. Phys. 14, 419 (1965).

3. J. Clarke, W.M. Goubau and M.B. Ketchen, J. Low Temp. Phys. 25, 99 (1976).

4. Claudia D. Tesche and John Clarke, J. Low Temp. Phys. 29, 301 (1977).

5. Roger Koch, D.J. Van Harlington and John Clarke, Appl. Phys. Lett. 38, (1981).

6. Gilbert Hawkings and John Clarke, J. Appl. Phys. 47, 1616 (1976).

7. Richard F. Voss and John Clarke, Phys. Rev. B13, 556 (1976).

8. M.B. Ketchen and C. C. Tsuei, to be published in the Proceedings of the 2nd International Conference on Superconducting Quantum Devices (held in West Berlin, May 1980).

9. R.H. Koch, D.J. Van Harlington and John Clarke, private communication.

10. Ho Jung Paik, Nuovo Cimento 55, 15 (1980).

11. C.D. Tesche, "A Novel Superconducting Magnetometer", final report submitted to NSF (#DAR-8009388) Feb. 1981.

12. W.C. Stewart, Appl. Phys. Lett. 12, 277 (1968) and D.E. McCumber, J. Appl. Phys. 39, 3113 (1968).

13. C.D. Tesche and J. Clarke, J. Low Temp. Phys., 37, 397 (1979).

14. Claudia D. Tesche, Ph.D. Thesis, University of California, Berkeley, (1978).

15. H.A. Kramers, Physica, 7, 284 (1940).

16. Patrick A. Lee, J. Appl. Phys. 42, 325, (1970).

17. J. Kurkijarvi, Phys. Rev., B6, 832 (1972).

18. T.A. Fulton, Phys. Rev., B7, 1189 (1973).

VII. REFERENCES (cont.)

19. T.A. Fulton, Phys. Rev., B9, 4760 (1974).

20. T.A. Fulton, IEEE Trans. Mag. vol. 11, pg. 749 (1975).

21. Herbert B. Callen and Theodore A. Welton, Phys. Rev., 83, 34 (1951).

22. D.R. Cox and P.A.W. Lewis, The Statistical Analysis of Series of Events, Chapter 4, (John Wiley and Sons, Inc., New York, 1966).

23. K.K. Likharev and V.K. Semenov, ZhETF Pis. Red., 15, 625 (1972).

24. M.G. Castellano and H.J. Paik, "Recent Experimental Work on Point-Contact DC SQUID" to be presented at LT-16, August 19-26, 1981 in Los Angeles, CA.

25. J. Clarke, C.D. Tesche, and R.P. Giffard, J Low Temp. Phys., 37, 405 (1979).

26. C.D. Tesche, "A Thermal Activation Model for the DC SQUID" to be published in J. Low Temp. Phys.

27. J.M. Jaycock and M.B. Ketchen, IEEE Trans. Mag. 17, 1.

28. B.A. Huberman, J.P. Crutchfield and N.H. Packard, Appl. Phys. Lett. 37, 750 (1980).

29. Y. Braiman, E. Ben-Jacob, Y. Imry in "SQUIDs and their Applications", H.D. Hahlbohm, eds. (1980) in press.

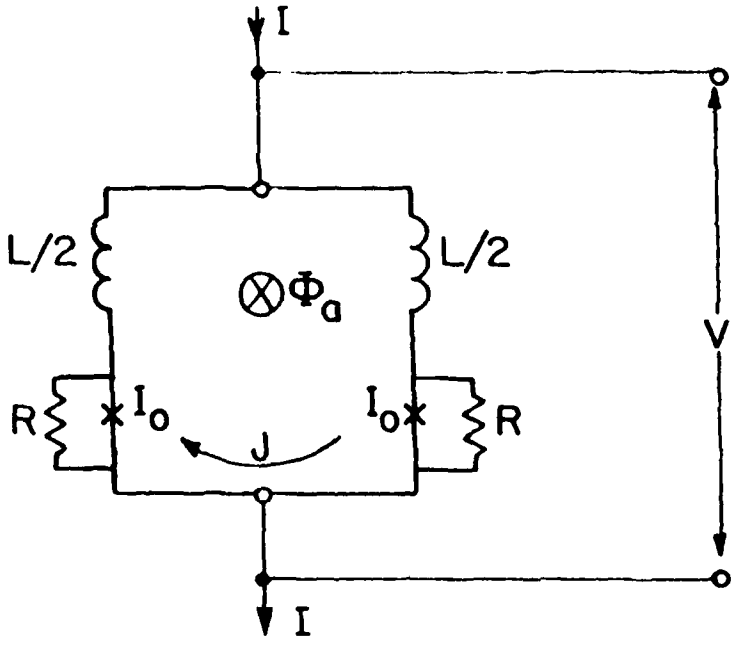

Figure 1. . Lumped Circuit Element Model for the DC SQUID.

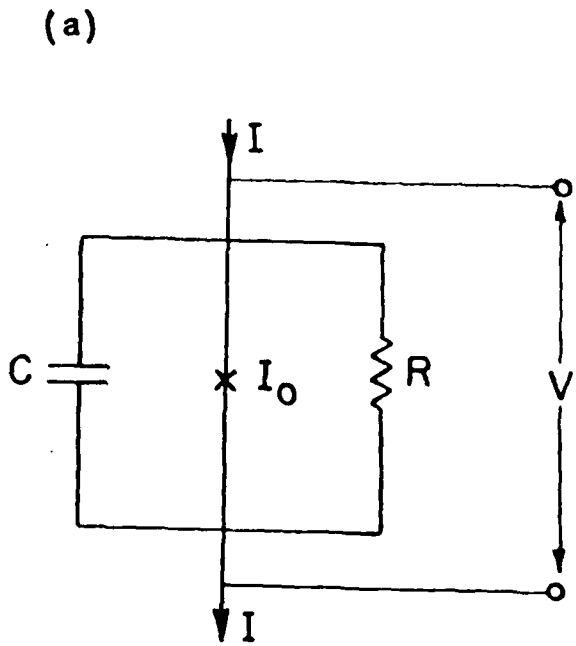

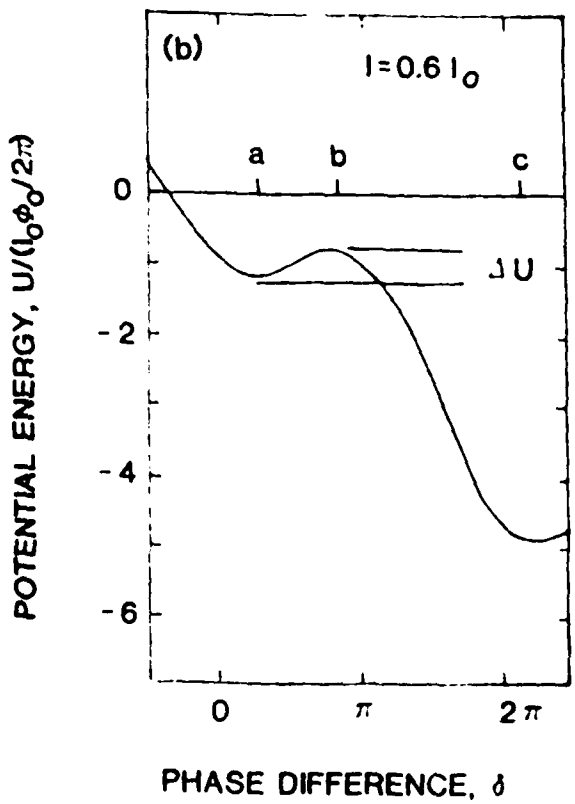

Figure 2. a) Resistively Shunted Junction Model (RSJ)
b) Washboard Potential.

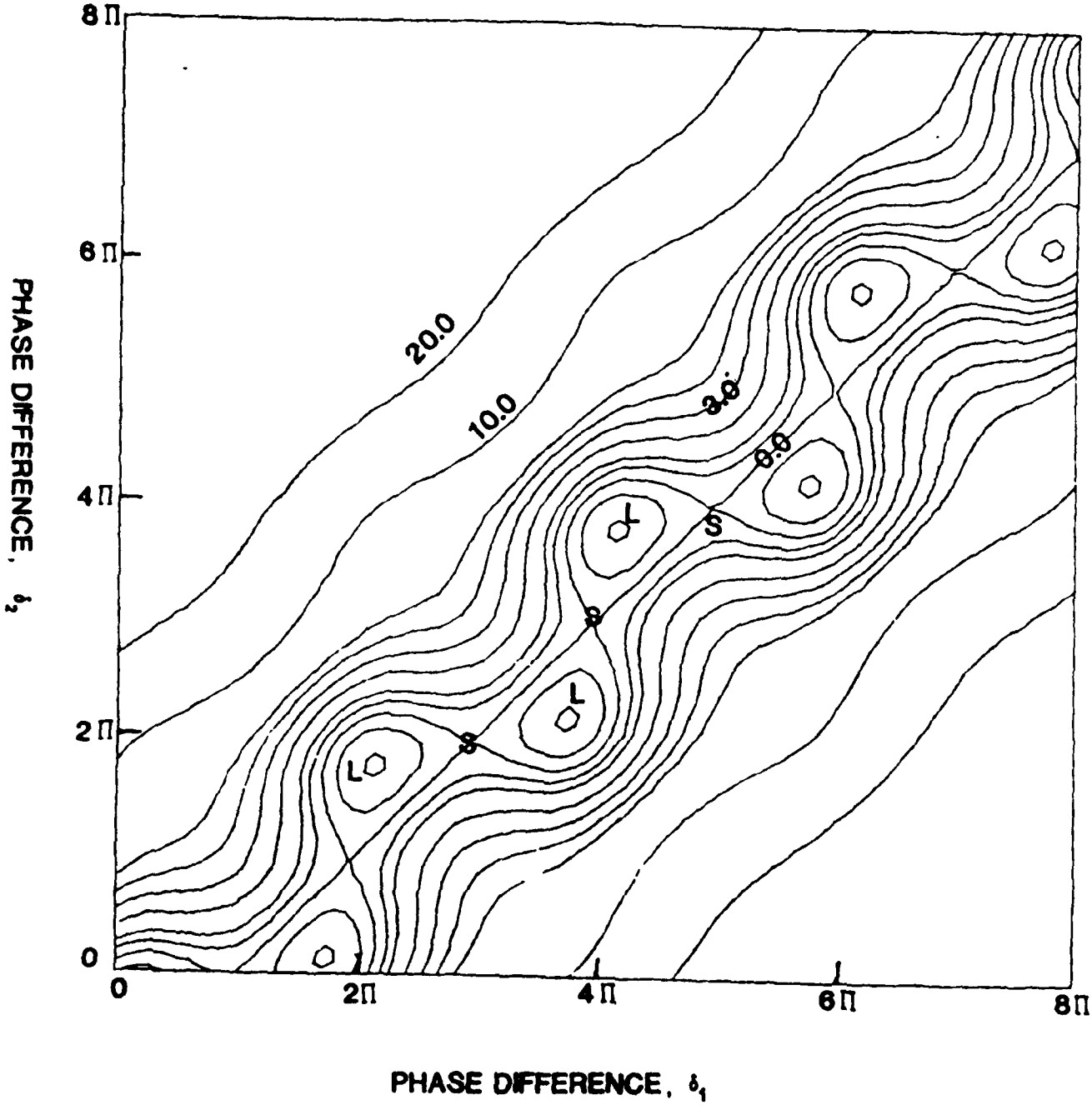

Figure 3. Contour Plot of Potential Energy for a DC SQUID with $I = 0$, $\Phi_a = \Phi_o/2$, $\beta = 1$.

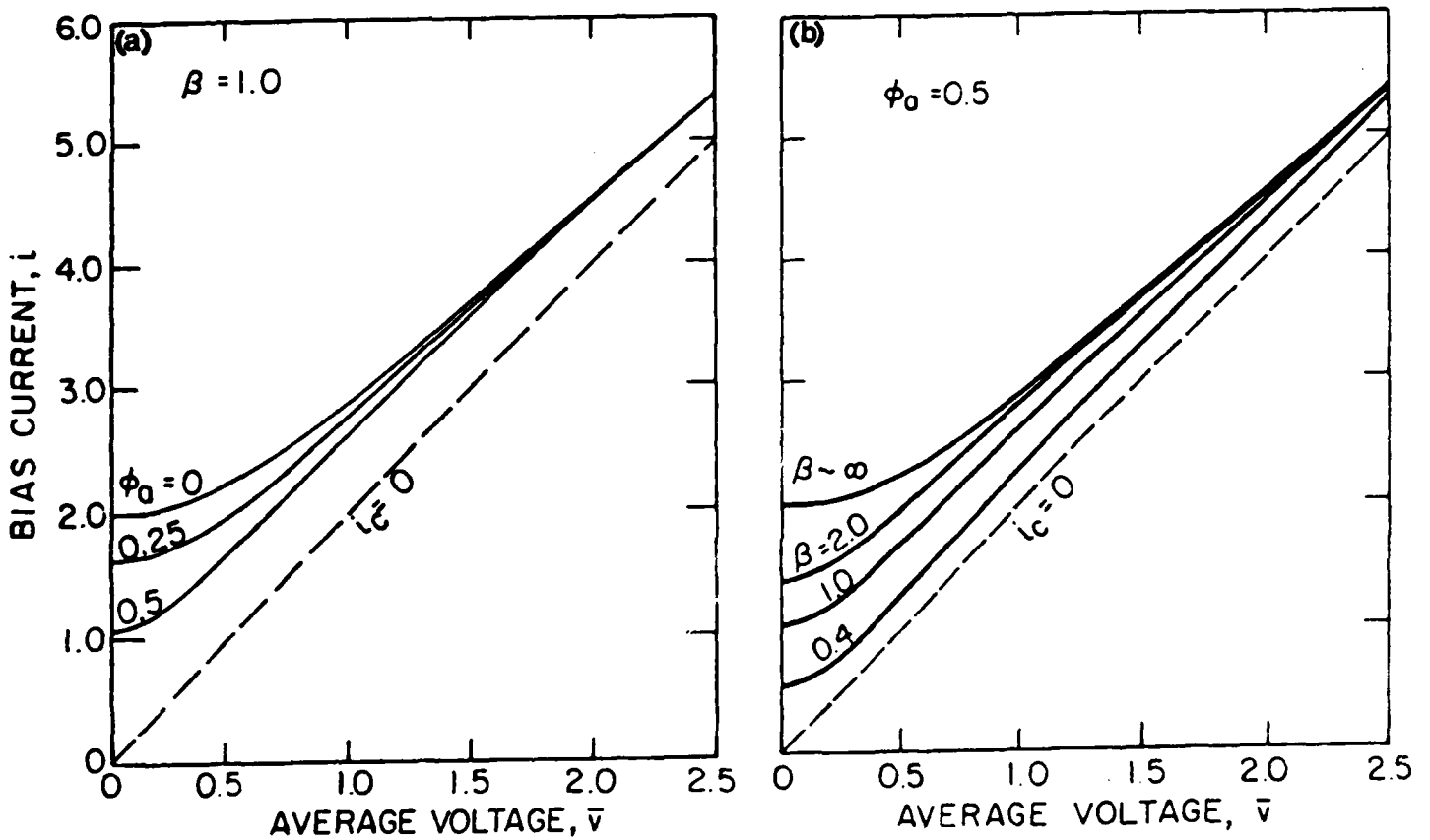

Figure 4. Noise Free I-V Characteristic for a Symmetric DC SQUID as a function of (a) applied flux and (b) β.

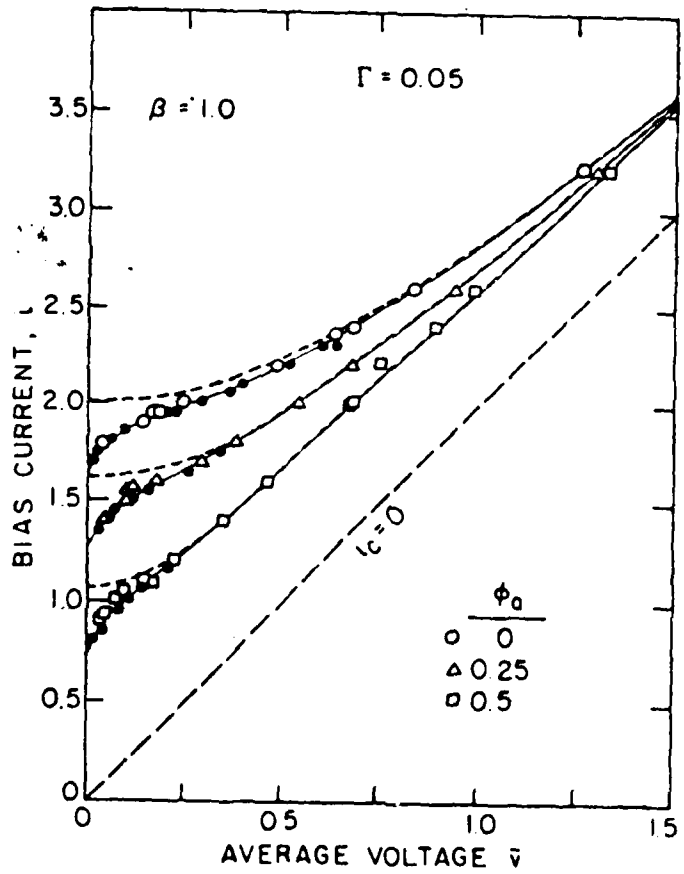

Figure 5. Noise Rounded I-V Characteristics for a DC SQUID as a Function of Applied Flux Φ_a.

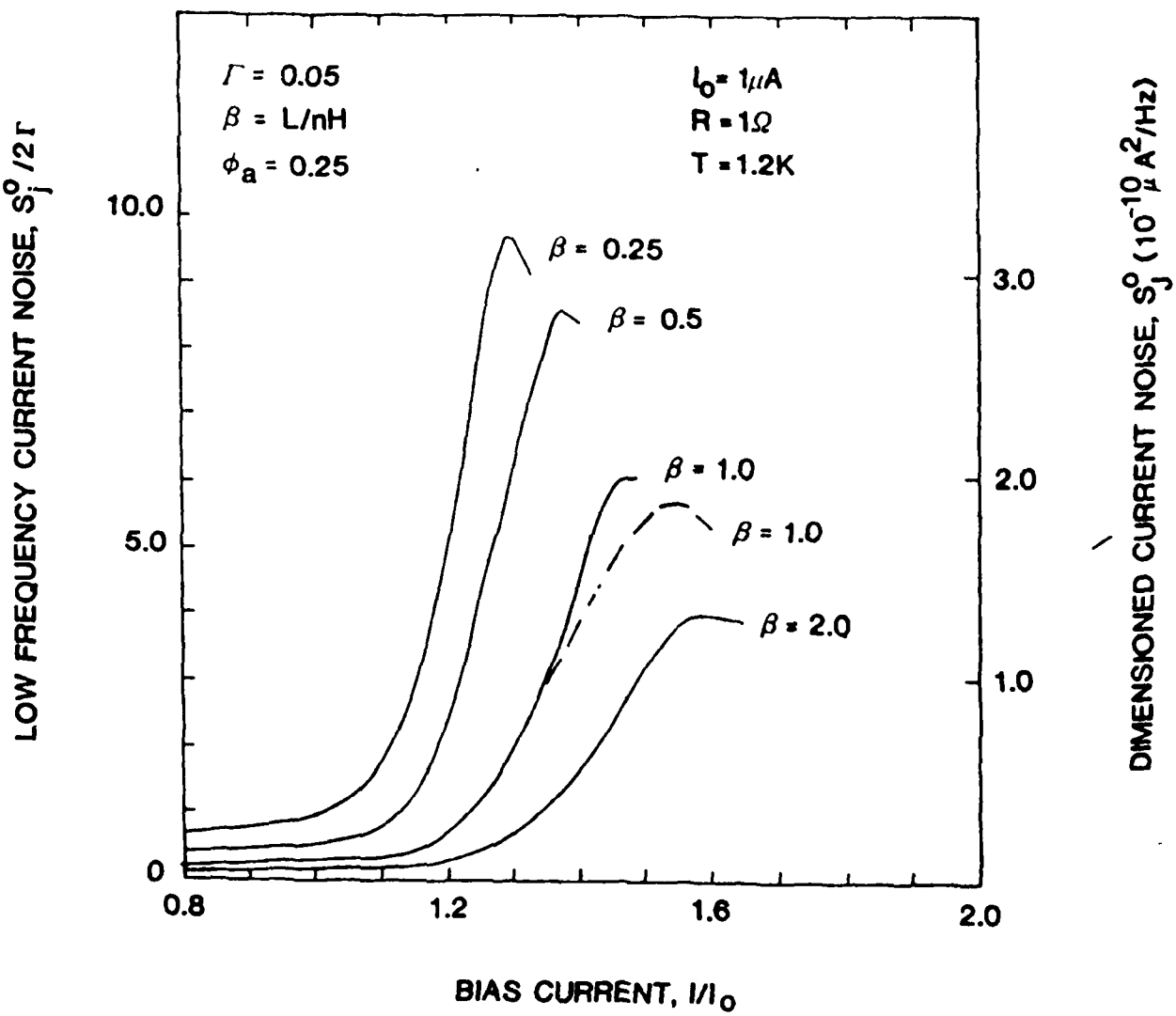

Figure 6. Low Frequency Circulating Noise Spectral Density, $S_j^o/2\Gamma$ Versus Bias Current I/I_o as a function of β for a DC SQUID.

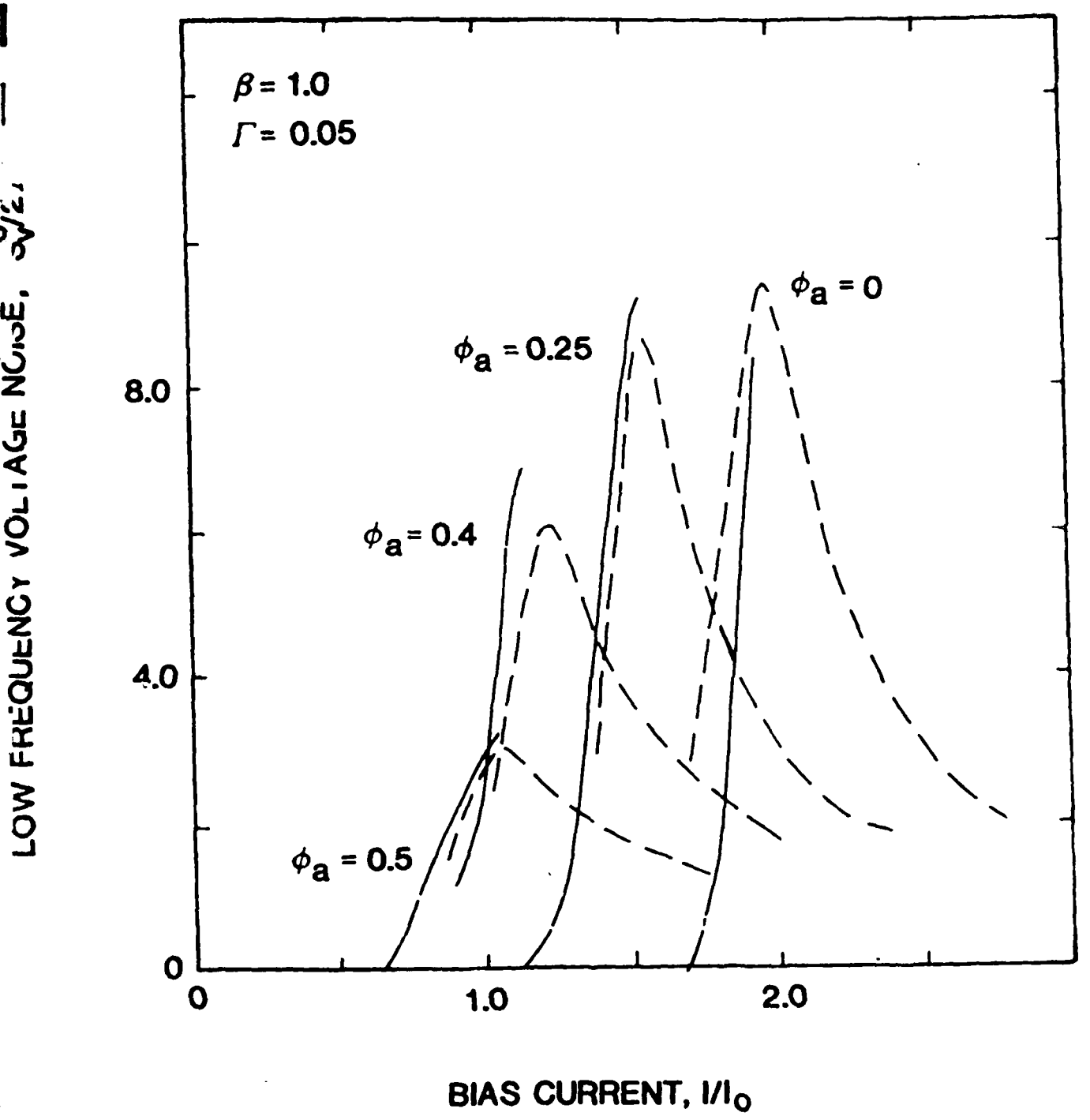

Figure 7. Low Frequency Voltage Noise Spectral Density $S_V^o/2\Gamma$ Versus Bias Current I/I_o as a function of applied flux, ϕ_a.

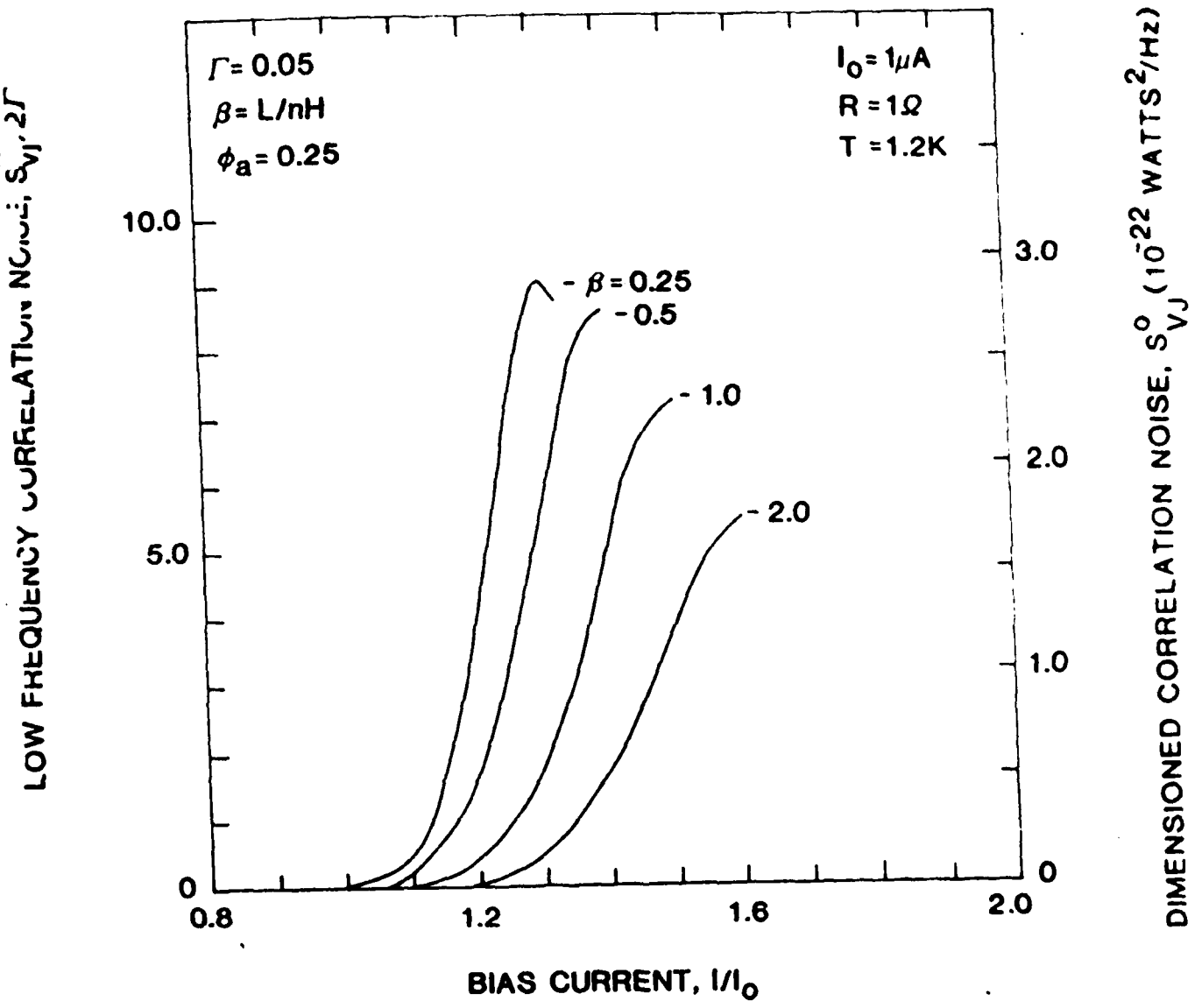

Figure 8. Low Frequency Correlation Spectral Density $S_{vj}/2\Gamma$ Versus Bias Current I/I_o as a function of .

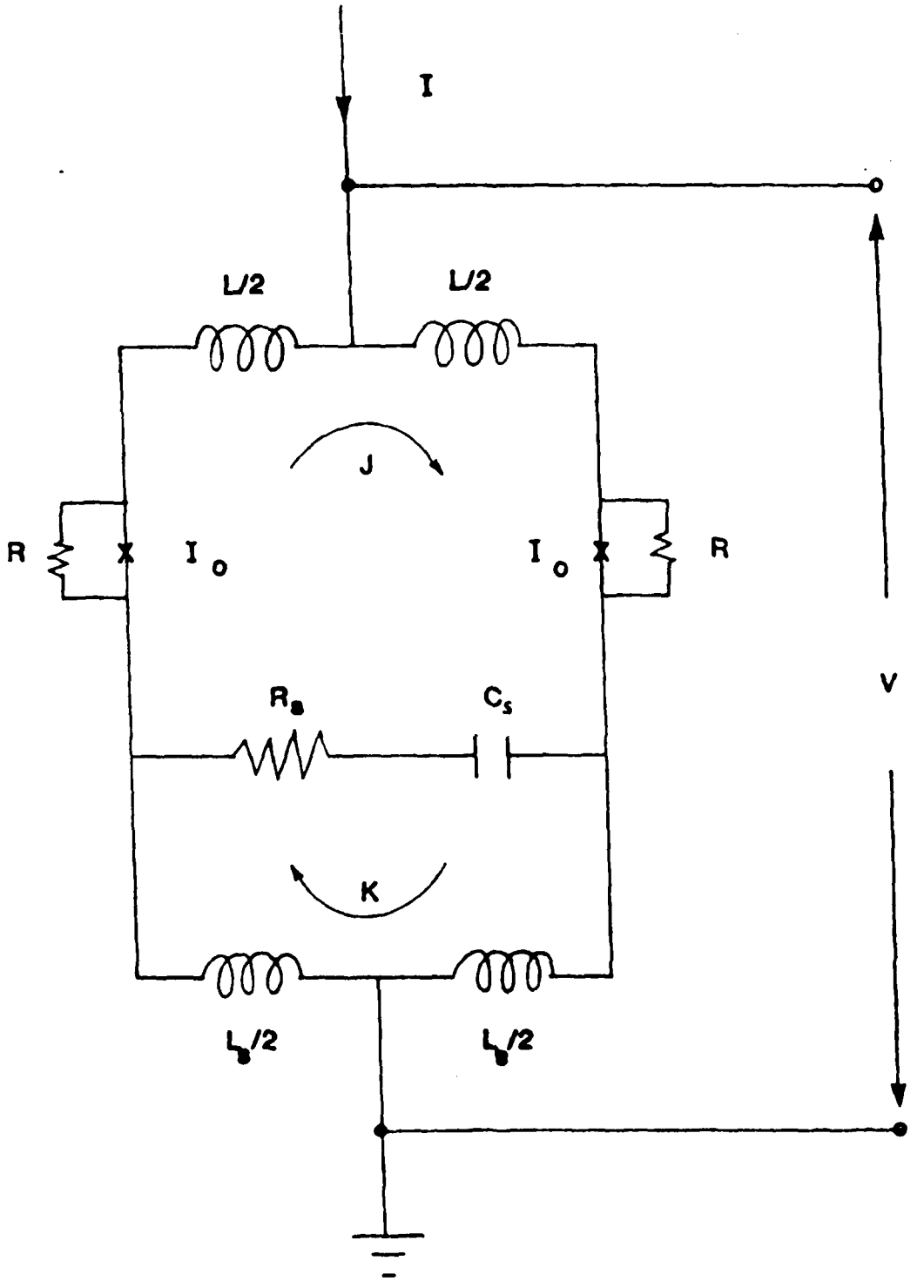

Figure 9. Lumped Circuit Element Model for the Double Loop SQUID.

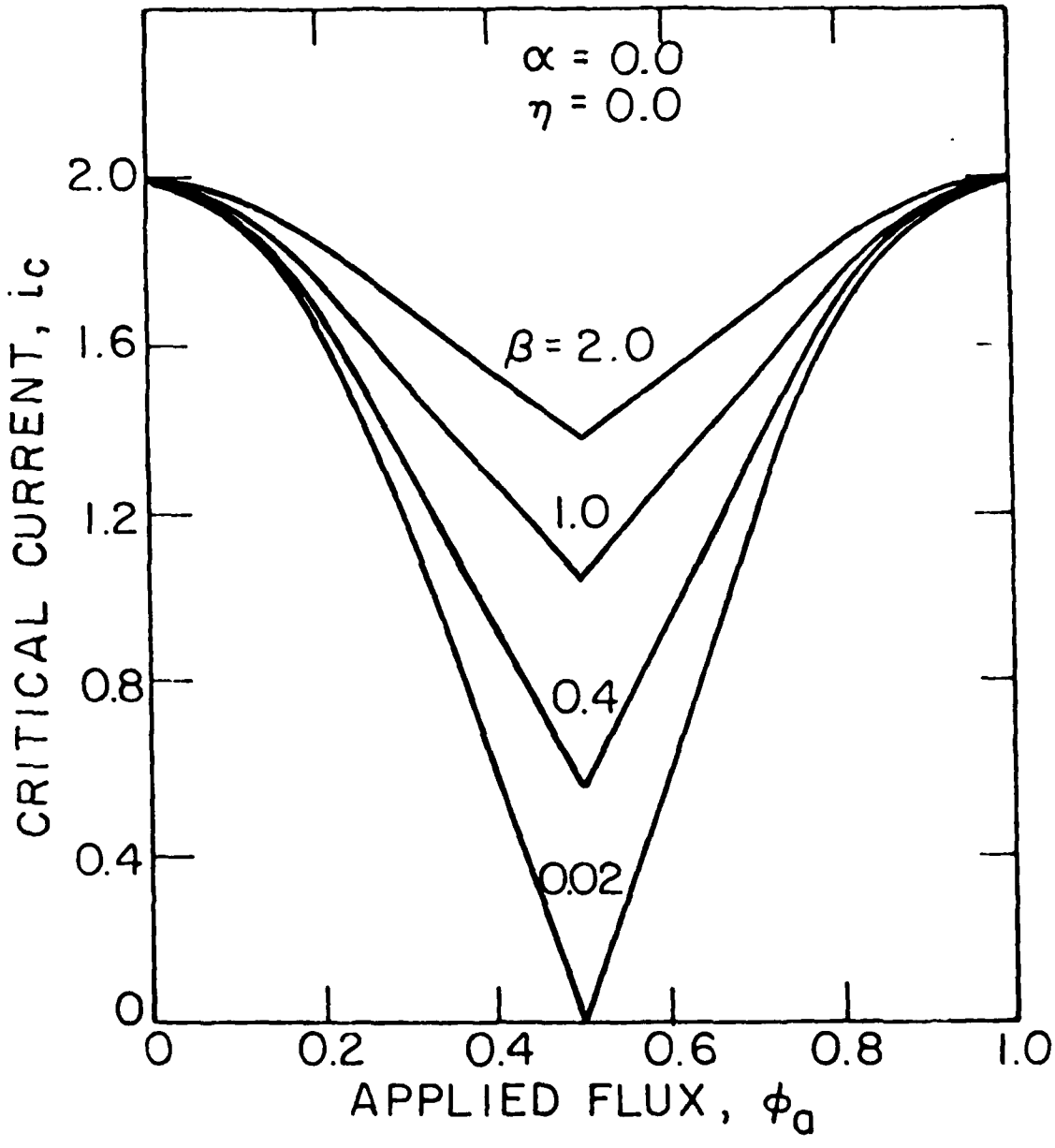

Figure 10. Critical Current, i_c, Versus Applied Flux, ϕ_a, as a function of β for the DC SQUID.

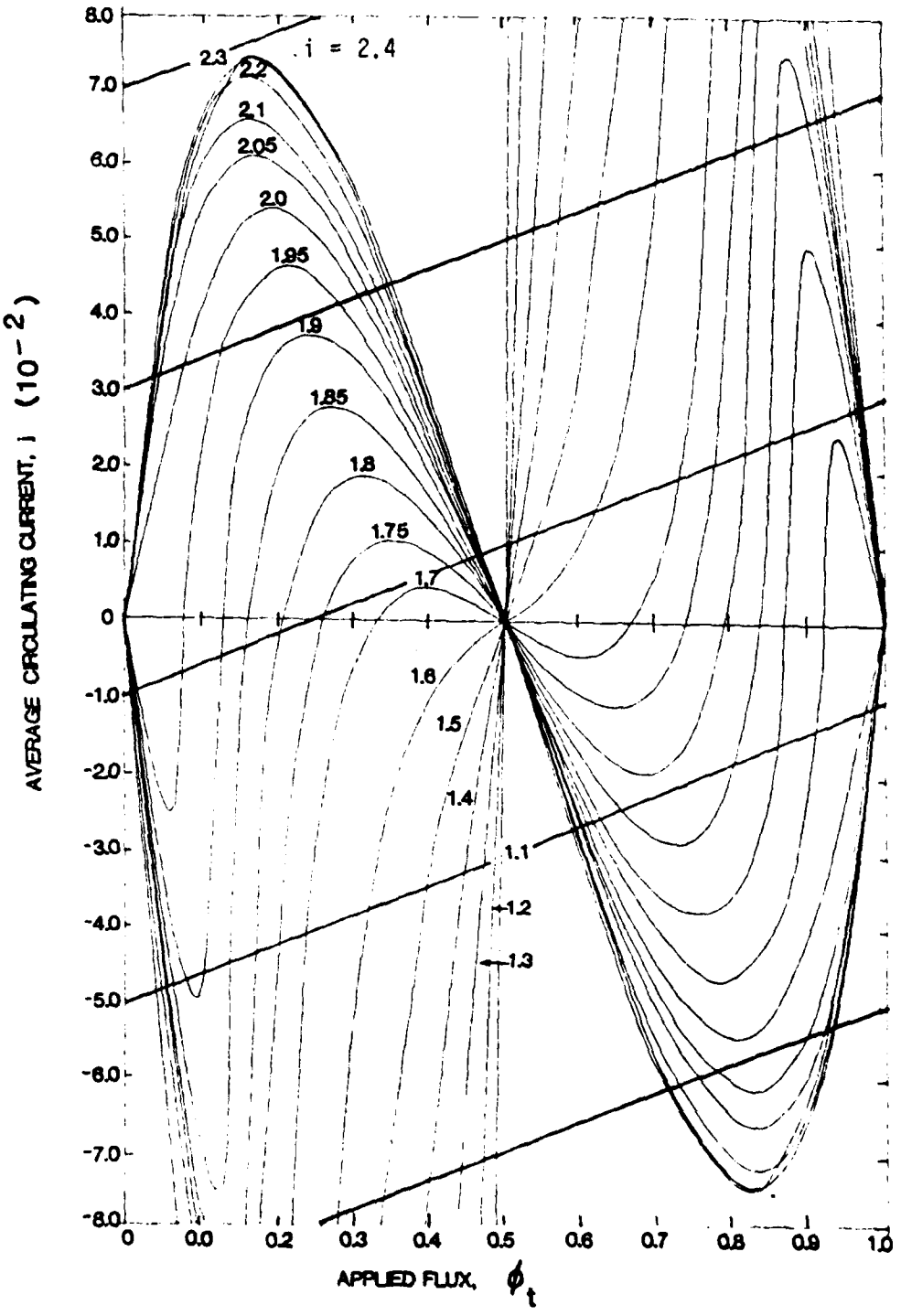

Figure 11. Average Circulating Current, <J> Versus Applied Flux, ϕ_T, as a function of bias current, i, for a DC SQUID with $\beta = 1$.

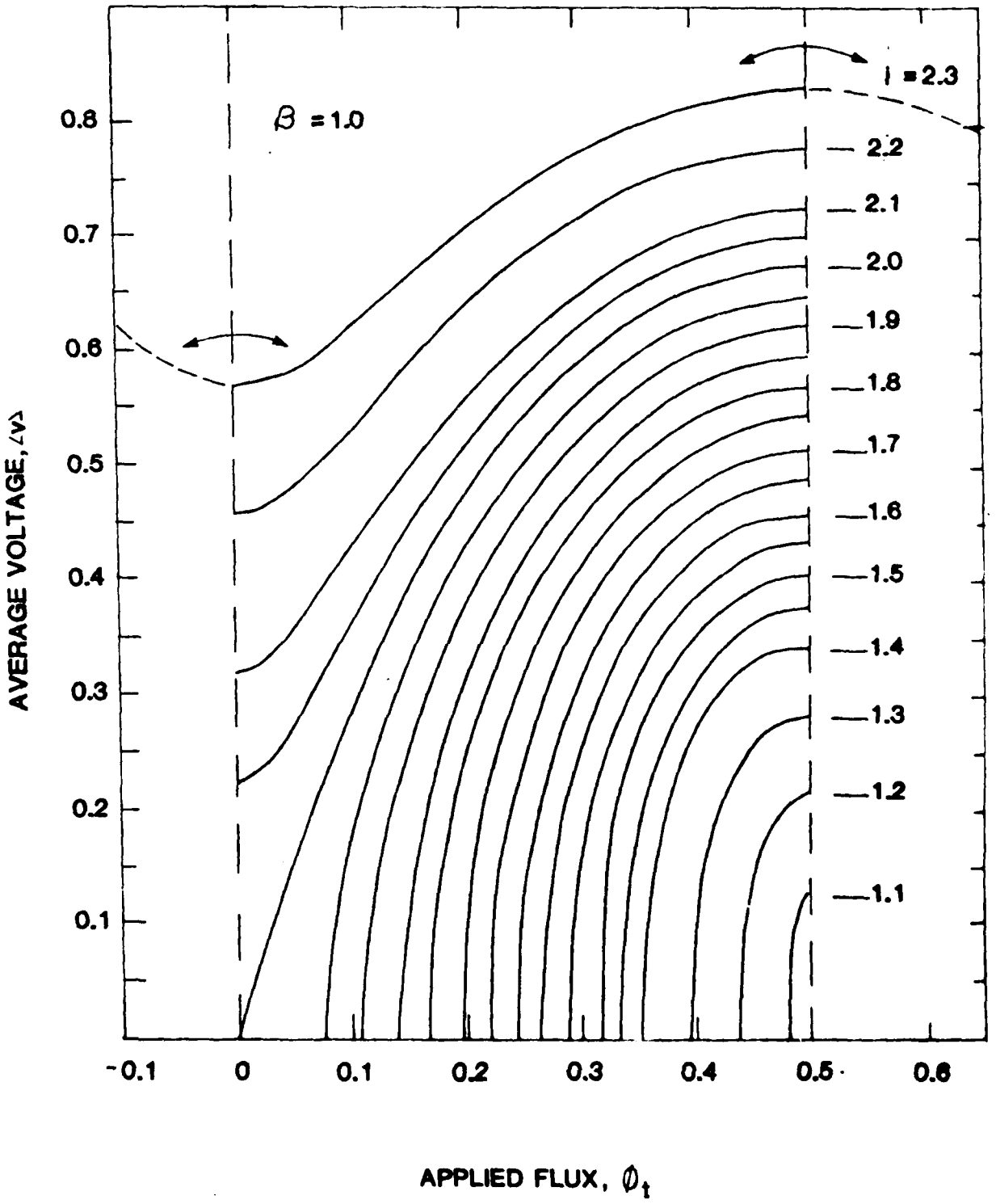

Figure 12. Average Voltage, $\langle v \rangle$, Versus Applied Flux, ϕ_T, for a DC SQUID with $\beta = 1$.

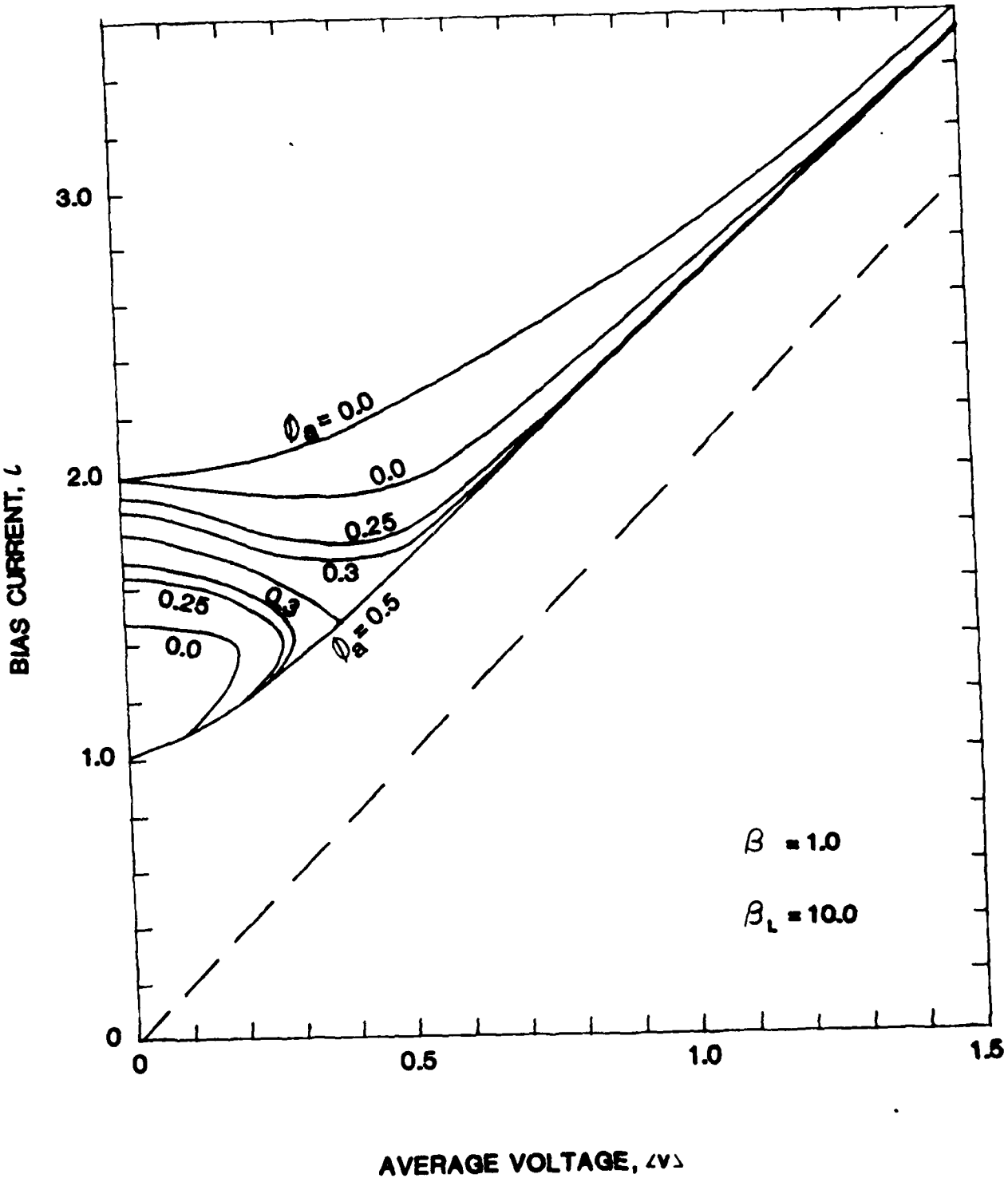

Figure 13. Noise Free I-V Characteristics for a Double Loop SQUID with $\beta = 1$, $\beta_L = 10$ as a Function of Applied Flux, ϕ_a.

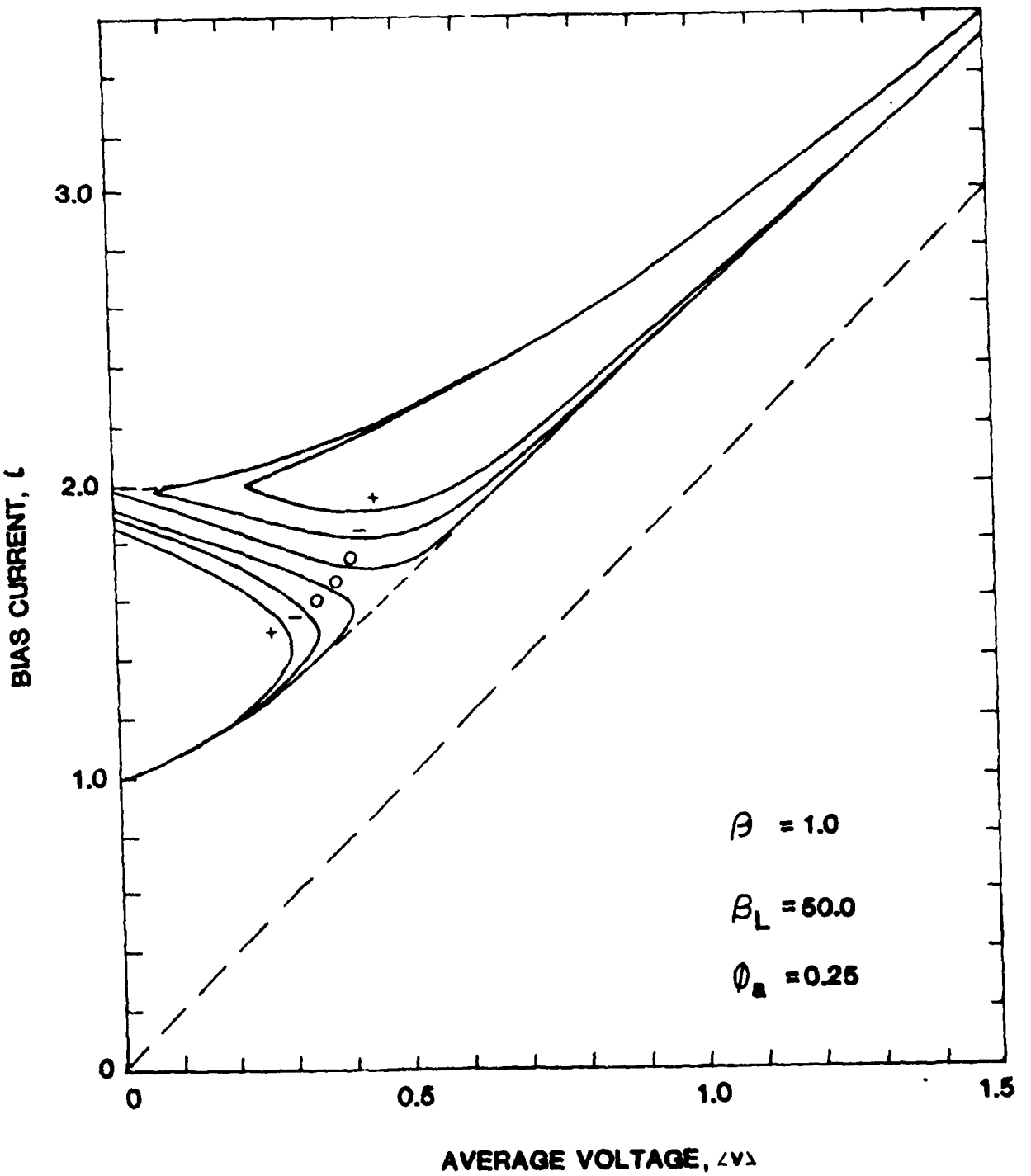

Figure 14. Noise Free I-V Characteristics for a Double Loop SQUID with $\beta = 1$, $\beta_L = 50$ and $\phi_a = 0.25$.

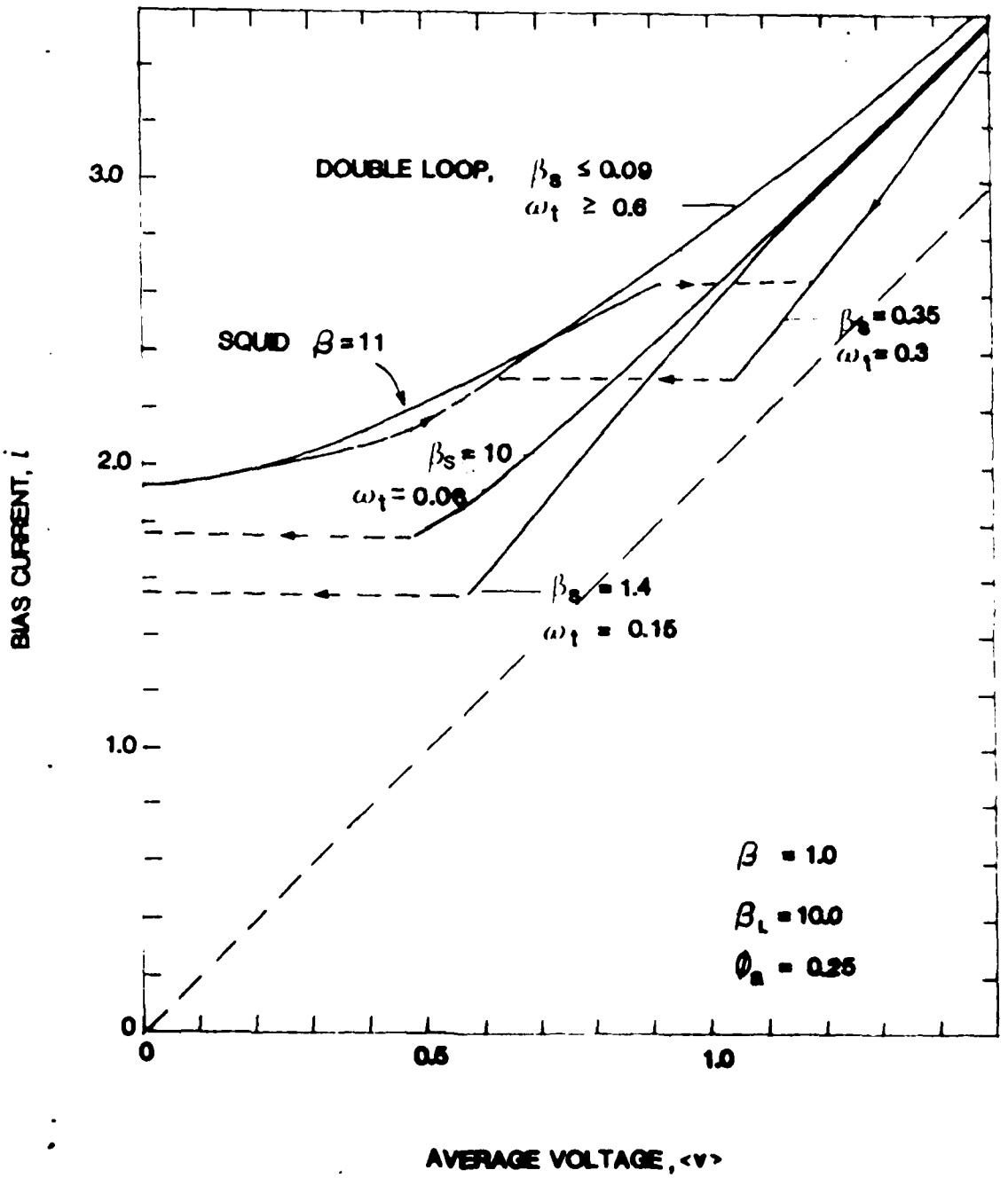

Figure 15. Noise Free I-V Characteristics for a Double Loop SQUID with $\beta = 1$, $\beta_L = 10$, and $\phi_a = 0.25$ as a function of the tank circuit frequency ω_t.

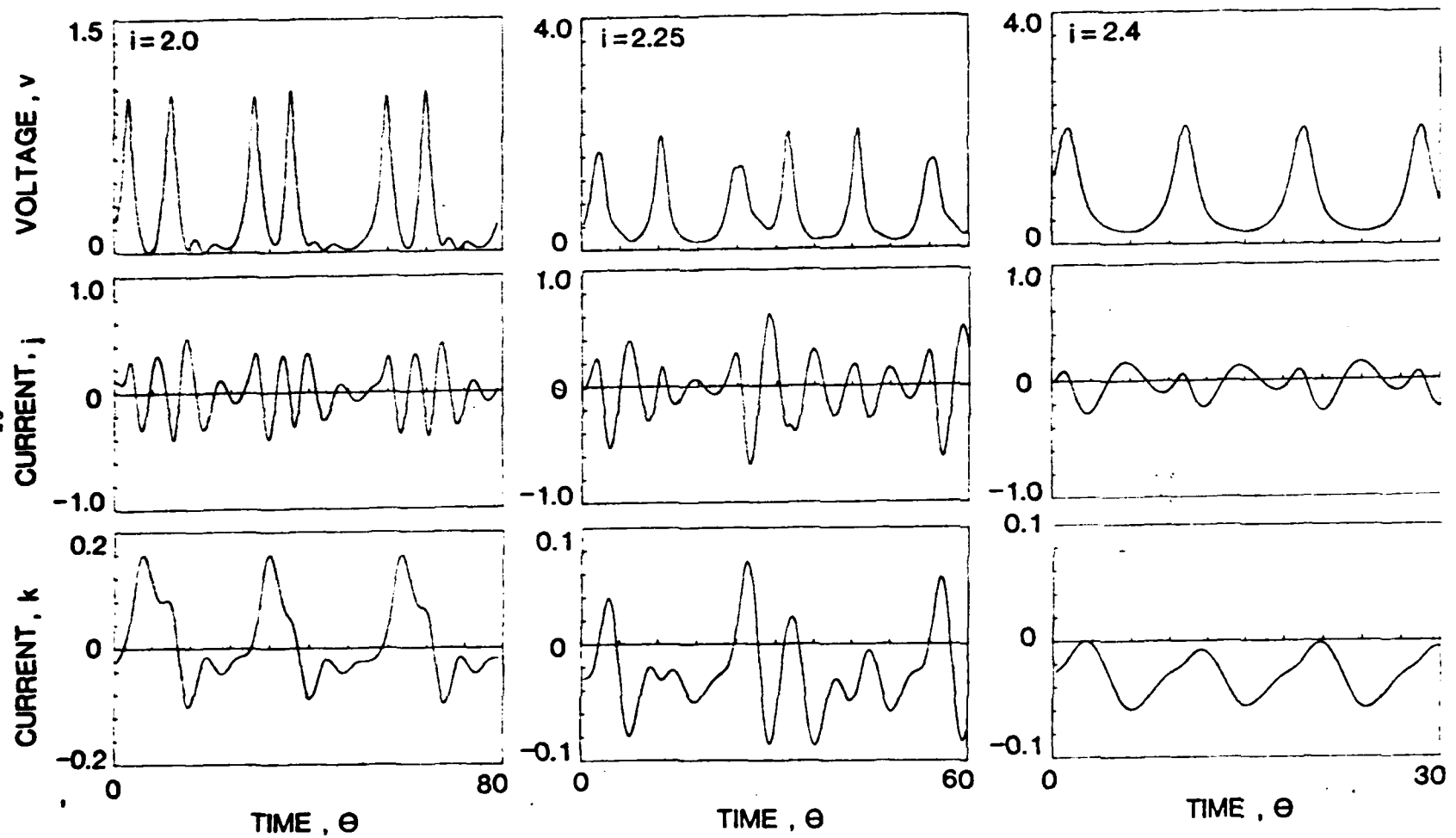

Figure 16. Plot of Voltage v, and Screening Currents k and j as a Function of Time, θ for a Double Loop SQUID with $\beta = 1$, $\beta_L = 10$, $\beta_C = 0.3537$, $\rho = 0.1$ and $i_a = 0.25$ for (a) Bias current

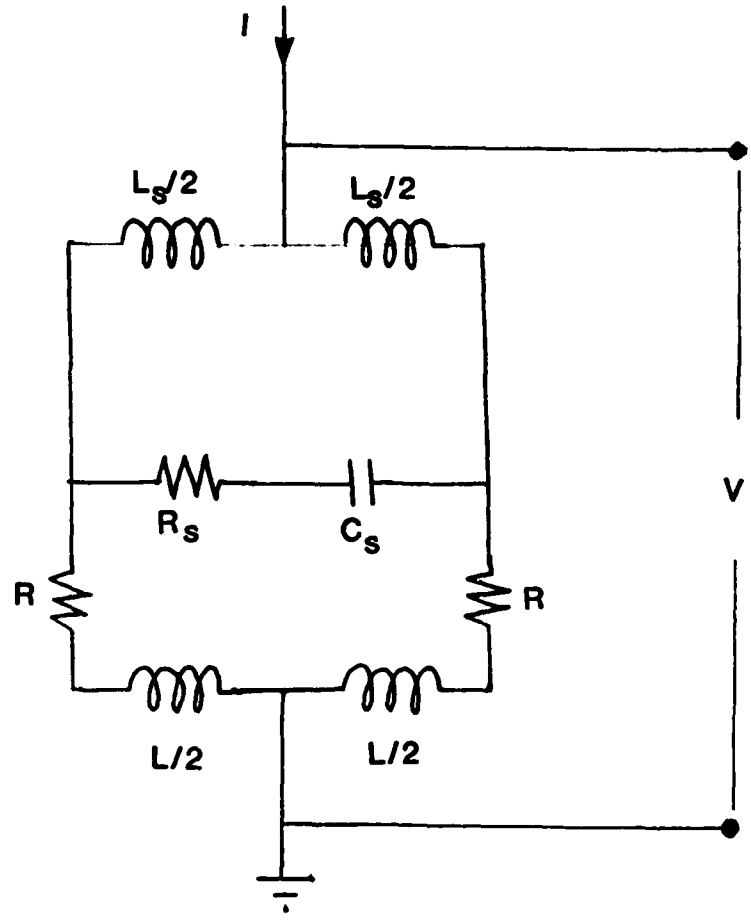

Figure 17. Plot of Equivalent Double Loop SQUID in the Limit $I_0 \to \infty$.

Figure 18. Noise Rounded I-V Characteristics, (b) Forward Transfer Function, (c)-(g) Low Frequency Noise Power Spectral Densities, and (h) Dimensionless Flux Noise as a Function of Bias Current for a Double Loop SQUID with $\beta = 1$, $\beta_L = 1$, $\beta_C = 100$, $\rho = 0.01$ and $\Gamma = 0.01$

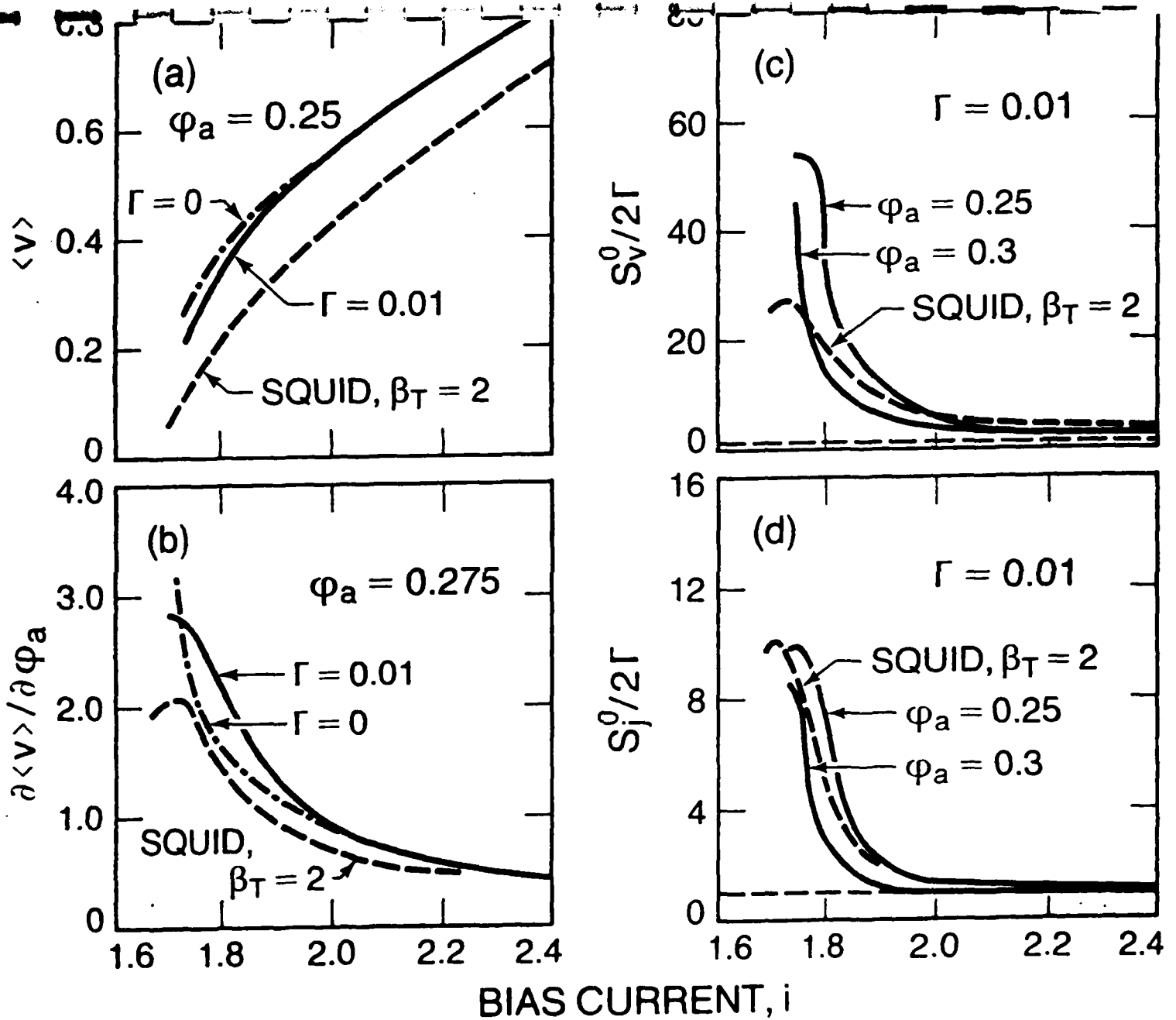
(a)
$\varphi_a = 0.25$
$\Gamma = 0$
$\Gamma = 0.01$
SQUID, $\beta_T = 2$
$\langle v \rangle$
(b)
$\varphi_a = 0.275$
$\Gamma = 0.01$
$\Gamma = 0$
SQUID,
$\beta_T = 2$
$\partial \langle v \rangle / \partial \varphi_a$
(c)
$\Gamma = 0.01$
$\varphi_a = 0.25$
$\varphi_a = 0.3$
SQUID, $\beta_T = 2$
$S_v^0/2\Gamma$
(d)
$\Gamma = 0.01$
SQUID, $\beta_T = 2$
$\varphi_a = 0.25$
$\varphi_a = 0.3$
$S_j^0/2\Gamma$
BIAS CURRENT, i

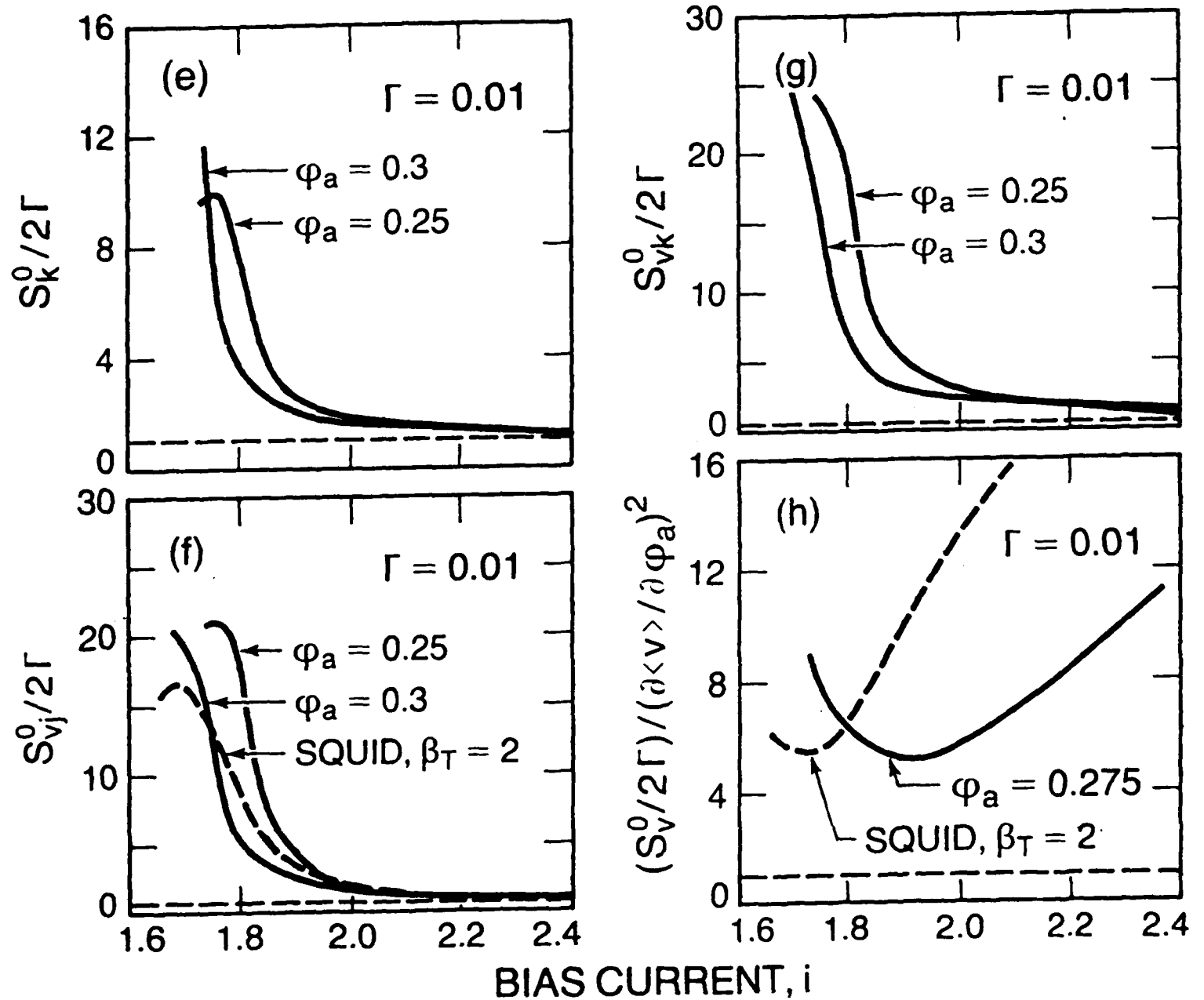
(e)
Γ = 0.01
φa = 0.3
φa = 0.25
$S^0_k/2\Gamma$
(f)
Γ = 0.01
φa = 0.25
φa = 0.3
SQUID, βT = 2
$S^0_{vj}/2\Gamma$
(g)
Γ = 0.01
φa = 0.25
φa = 0.3
$S^0_{vk}/2\Gamma$
(h)
Γ = 0.01
φa = 0.275
SQUID, βT = 2
$(S^0_v/2\Gamma)/(\partial\langle v\rangle/\partial\varphi_a)^2$
BIAS CURRENT, i

Figure 19. Noise Rounded I-V Characteristics, (b) Forward Transfer Function, (c)-(g) Low Frequency Noise Power Spectral Densities, and (h) Dimensionless Flux Noise as a Function of Bias Current for a Double Loop SQUID with $\beta = 1$, $\beta_L = 10$, $\beta_C = 10$, $\rho = 0.1$ and $\Gamma = 0.001$.

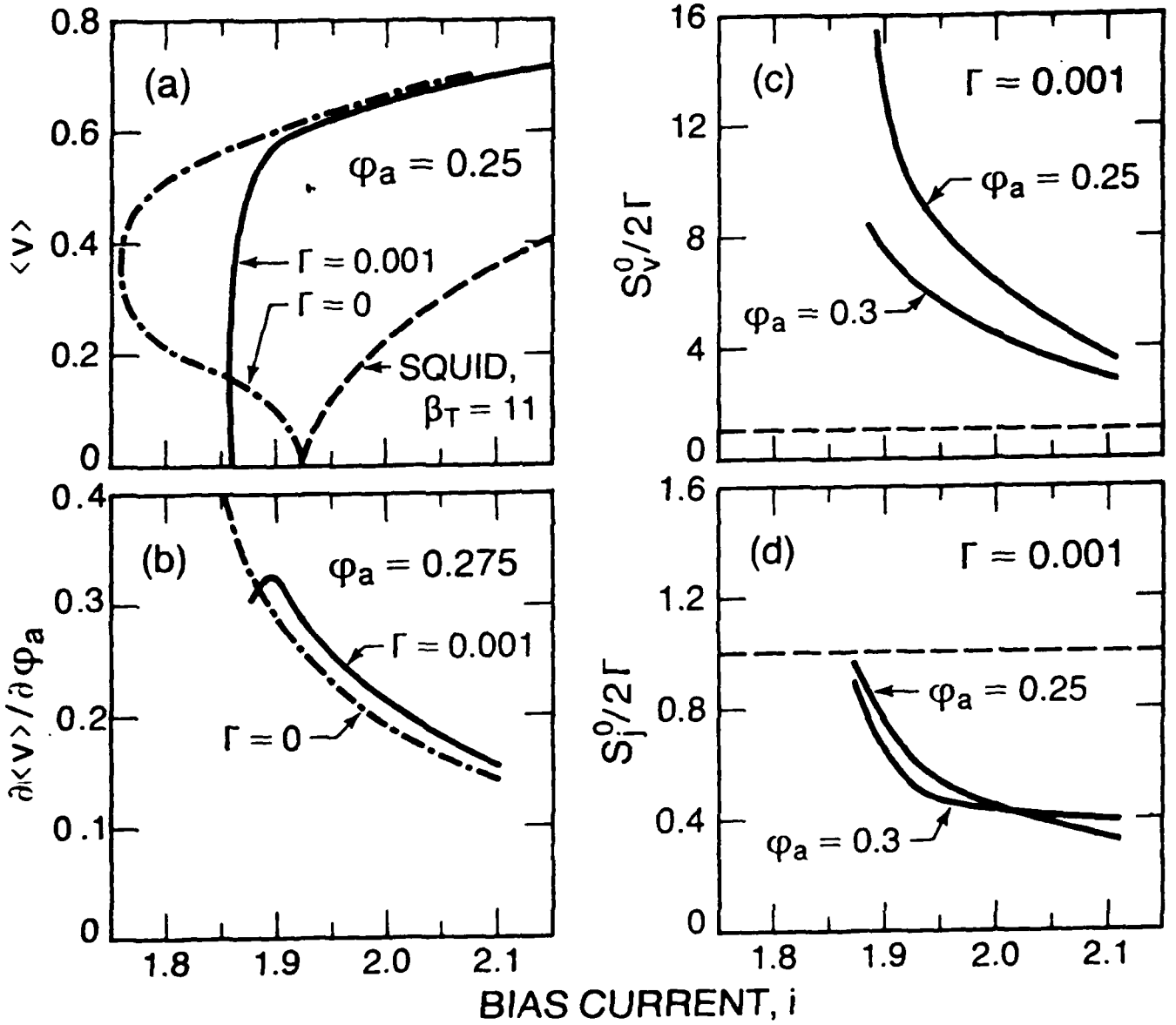
(a)
(b)
(c)
(d)
$\varphi_a = 0.25$
$\varphi_a = 0.275$
$\varphi_a = 0.3$
$\Gamma = 0.001$
$\Gamma = 0$
SQUID,
$\beta_T = 11$
$\langle v \rangle$
$\partial \langle v \rangle / \partial \varphi_a$
$S_v^0 / 2\Gamma$
$S_j^0 / 2\Gamma$
BIAS CURRENT, i

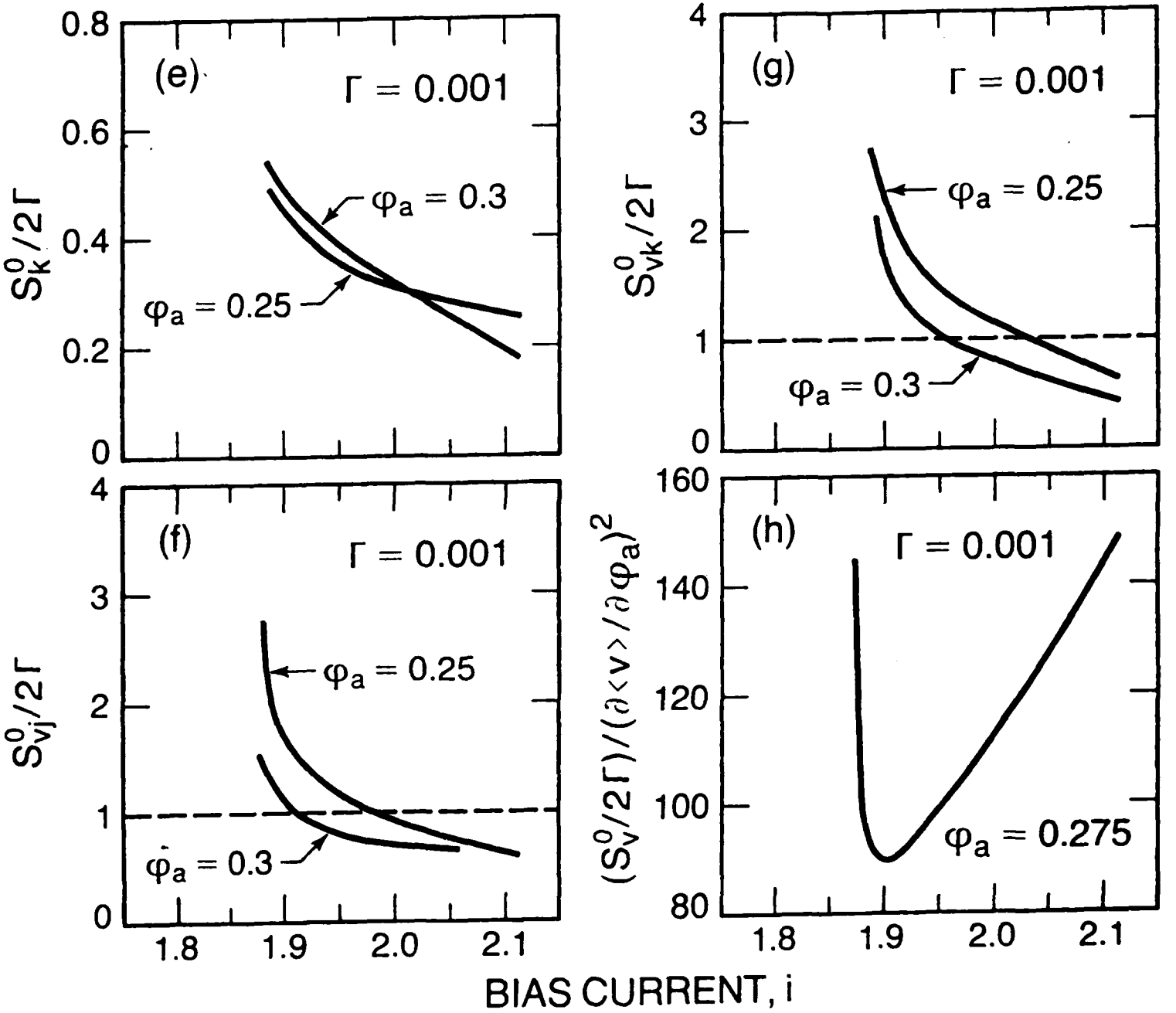
(e)
Γ = 0.001
$\varphi_a = 0.3$
$\varphi_a = 0.25$
$S_k^0/2\Gamma$
0.8
0.6
0.4
0.2
0
(g)
Γ = 0.001
$\varphi_a = 0.25$
$\varphi_a = 0.3$
$S_{vk}^0/2\Gamma$
4
3
2
1
0
(f)
Γ = 0.001
$\varphi_a = 0.25$
$\varphi_a = 0.3$
$S_{vj}^0/2\Gamma$
4
3
2
1
0
(h)
Γ = 0.001
$\varphi_a = 0.275$
$(S_v^0/2\Gamma)/(\partial\langle v\rangle/\partial\varphi_a)^2$
160
140
120
100
80
1.8
1.9
2.0
2.1
BIAS CURRENT, i

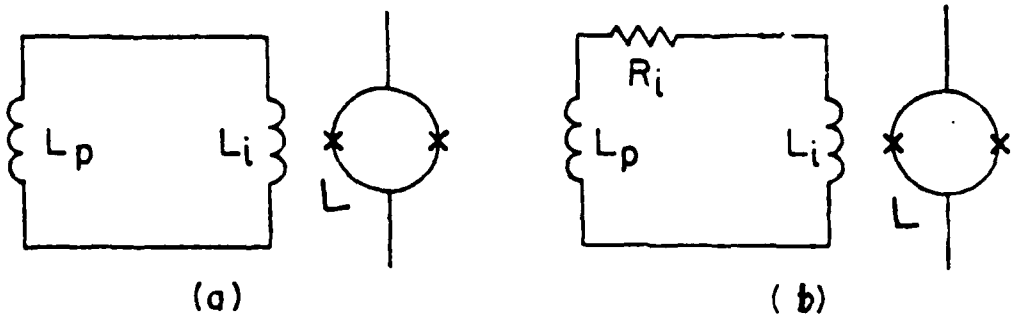

Figure 20. DC SQUID Magnetometer with
(a) Superconducting Input Circuit and
(b) Lossy Input Circuit.

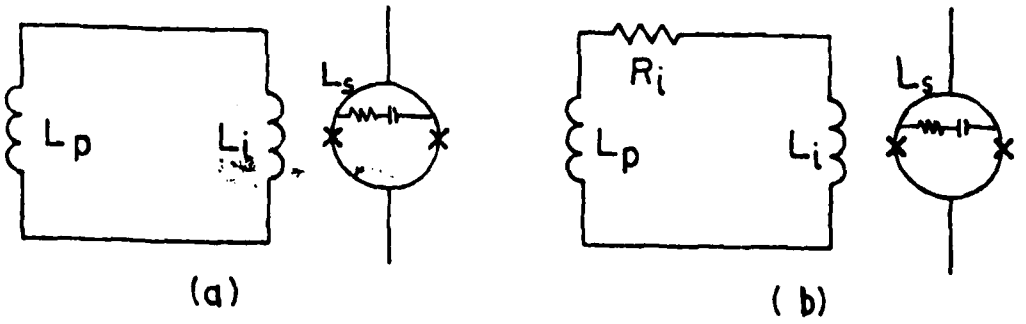

Figure 21. Double Loop SQUID Magnetometer System with
(a) Superconducting Input Circuit
(b) Lossy Input Circuit.


DATE
ILME